AIRBUS

DEFENCE AND SPACE

ALBA: ADVANCED L-BAND ANTENNA FOR NG SMOS MISSIONS

ALBA-ADSM-TN-1002028381, Issue 01, Date: 04/12/2024

L-Band Antenna for Next Generation SMOS Missions (ALBA) Executive Summary

DRL Reference:	**N/A**	Category:	**N/A**
C.I. Number:	**0000**	No. of pages:	**67**
Model:	**all**		

Prepared by	Revised by	Approved by
ALBA Project Team	**Ana Lopez-Yela; Albert Zurita; Quiterio Garcia; Ana Olea**	**Ana Olea** Ana Olea García Firmado digitalmente por Ana Olea García Fecha: 2024.12.09 15:08:30 +01'00'

Export Control Information

This document contains national, EU or/and US export controlled technology (data):

Yes ☐ **No** ☒

If No:

This document has been assessed against all applicable export control regulations and is **"Not Listed".**

If Yes, please complete the following as applicable:

1/ National Military / Dual-use export controlled content

(other than US and UK)

Country/countries of origin for technology contained in this document:

☐ France ☐ Germany ☐ Spain ☐ other: [specify country]

☐ This document contains technology which is controlled by military export control regulation, classification [e.g. MLXXX / AMAXX]. Transmission abroad requires an export licence.

☐ This document contains technology which is controlled by national dual-use regulation, classification [XEXXX], or by European Union dual-use regulation 428/2009 Annex IV as amended, classification [XEXXX]. Transmission abroad requires an export licence.

☐ This document contains technology which is controlled by European Union dual-use regulation 428/2009 Annex I as amended, classification [XEXXX]. Transmission within the EU does not require an export licence. Export from the EU requires an export licence.

2/ UK Export Controlled content

☐ This document contains technology which has been assessed against the UK Export Control list and is rated as [e.g. MLXXX / XEXXX]. Transfer from the UK requires an export licence.

3/ US (ITAR / EAR) export controlled content

☐ This document contains technology which is controlled by the U.S. government under [USML category number / ECCN] and which has been received by [legal entity] under authority of [licence number / ITAR exemption / EAR licence exception / NLR]. Any re-export or re-transfer of this document in part or in whole must be made in accordance with the appropriate regulation (ITAR/EAR) and authorization (e.g. DSP 5, TAA, ITAR exemption, BIS licence or licence exception, NLR).

☐ This document contains technology which is designated as EAR99 (subject to EAR and not listed on the CCL).

DISTRIBUTION LIST		
INTERNAL	**EXTERNAL**	
Name	**Co.**	**Name**
ALBA ASE Team	ESA	Erio GANDINI
	ESA	Manuel MARTÍN-NEIRA
	ESA	Martín SUESS

ISSUE RECORD					
Issue	**Date**	**Nr.**	**Chapter**	**Description of Changes**	**Impact on the Product**
01	4/12/2024	--	--	Initial Issue	N/A

TABLE OF CONTENTS

1. SCOPE 10
2. APPLICABLE AND REFERENCE DOCUMENTS 11
2.1 APPLICABLE DOCUMENTS 11
2.2 REFERENCE DOCUMENTS 11
2.3 ACRONYMS 11
2.4 PAPERS PUBLISHED 12
3. INTRODUCTION 13
4. BACKGROUND OF THE PROJECT 14
5. ALBA ANTENNA 17
5.1 RADIATING ELEMENT DESCRIPCION 17
5.2 TRIHEX SPACECRAFT INSTRUMENT CONFIGURATION 20
6. SIMULATION RESULTS 22
6.1 INDIVIDUAL ANTENNA ANALYSIS 22
6.2 TRIHEX ARRAYED ANTENNA ANALYSIS 23
7. ALBA ANTENNA ELEMENTS TEST CAMPAIGN RESULTS 30
7.1 SINGLE ELEMENT RESULTS 31
7.1.1 T1 dimensional testing, mass 31
7.1.1.1 Dimensional Testing 31
7.1.1.2 Mass 31
7.1.2 T2: S parameter Test (individuals) 32
7.1.2.1 Conclusions 32
7.1.3 T3: Radiation Pattern Test (Individuals) 34
7.1.3.1 Radiation Pattern Measurements 35
7.1.3.2 Deviation masks 38
7.1.3.3 Efficiency Measurements 40
7.1.3.4 Conclusions 41
7.1.4 T4 S-Parameter Vs Temperature (2 individuals) 42
7.1.4.1 Conclusions 43
7.1.5 T5: Insertion Amplitude/Phase Vs Temperature 43
7.1.5.1 Conclusions 44
7.1.6 Single Element Conclusion 44
7.2 ALBA ARRAY BREADBOARD 45
7.2.1 T7: Scattering parameters results over temperature 45

7.2.1.1 Coupling terms in temperature range (-10ºC to +40ºC) 47
7.2.1.2 V-V coupling terms 48
7.2.1.3 H-H coupling terms 48
7.2.1.4 V-H coupling terms 49
7.2.1.5 H-V coupling terms 49
7.2.1.6 Conclusions 50
7.2.2 T8 array embedded element patterns 51
7.2.2.1 Radiation Pattern Measurements 52
7.2.2.2 Deviation Masks 55
7.2.2.3 Efficiency Measurements 57
7.2.2.4 Array Breadboard Conclusions 58
8. INSTRUMENT PERFORMANCES 60
8.1 SYSTEM SIMULATOR DESCRIPTION 60
8.2 IMAGE RECONSTRUCTION RESULTS 61
8.2.1 Error-free antenas 62
8.2.2 Antenas with measurement errors 63
9. FINAL CONCLUSIONS AND ACHIEVED RESULTS 64
10. COMPLIANCE MATRIX 65

FIGURES

FIGURE 4-1: PHOTOGRAPH OF ASSEMBLED ANTENNA MODEL 14
FIGURE 4-2: DEFINITION OF TRIHEX-SMOS RADIATING SUBSYSTEM WITH RADIATING ELEMENTS USED IN THE BB OF THE ANTENNA INSTRUMENT 15
FIGURE 4-3: DEFINITION OF ALBA-TRIHEX BREADBOARD. 16
FIGURE 5-1: 3D VIEWS OF THE ANTENNA CAVITY 17
FIGURE 5-2: 3D VIEW OF THE FEED NETWORK FOR THE ANTENNA 18
FIGURE 5-3: GEOMETRY OF THE ANTENNA STRUCTURE FOR INTEGRATION IN THE HEXAGONAL TRIHEX INSTRUMENT 19
FIGURE 5-4: 3D CROSS-SECTION OF THE SMOS ALBA ANTENNA 19
FIGURE 5-5 ALBA ANTENNA ELEMENT WITH CLOSING GASKET (PROVIDED BY LEADER TECH) 20
FIGURE 5-6 RELATIVE ORIENTATIONS OF THE RADIATING ELEMENTS IN THE RADIATING APERTURE OF TRIHEX. EACH COLOUR INDICATES A DIFFERENT POLARIZATION ORIENTATION RESPECT A COMMON VIEW POINT. 21
FIGURE 6-1: ANTENNA MESHING FOR SIMULATION IN CST. 22
FIGURE 6-2: S-PARAMETER PERFORMANCE IN SIMULATION FOR THE INDIVIDUAL ANTENNA AT THE EDGE OF THE GROUND PLANE. 22
FIGURE 6-3:RADIATION PATTERN SIMULATED PERFORMANCES AT THE CENTRE FREQUENCY, LEFT) VERTICAL POLARIZACION AND RIGHT) HORIZONTAL POLARIZATION. 23
FIGURE 6-4:·3D EM MODEL TO CHARACTERIZE THE TRIHEX CONFIGURATION 24
FIGURE 6-5: COUPLING TERMS (H-H, V-V, H-V AND V-H) FOR THE CENTRAL ELEMENT OF THE ARM (E7). 25
FIGURE 6-6:COPOLAR AND CROSSPOLAR COMPONENT FOR ELEMENTS E1-E13 AT PHI 0,45 AND 90 DEGREES, LEFT)FOR HORIZONTAL POLARIZATION AND RIGHT) FOR VERTICAL POLARIZATION 26
FIGURE 6-7: COPOLAR AND CROSSPOLAR COMPONENT FOR ELEMENTS E1-E13 AT PHI 0,45 AND 90 DEGREES 27
FIGURE 7-1: MEASURED S-PARAMETERS FOR EACH SN ANTENNA FOR VERTICAL POLARIZATION (S11) AND HORIZONTAL POLARIZATION (S22). 32
FIGURE 7-2: MEASURED S-PARAMETERS FOR DIFFERENT PATCH DIAMETER IN VERTICAL POLARIZATION (J1) (S11) AND HORIZONTAL POLARIZATION (J2) (S22), AND PORT COUPLING (S21). 33
FIGURE 7-3: ANTENNA LOCATED AT THE EDGE OF THE GROUND PLANE 34
FIGURE 7-4 ANTENNA ELEMENT PORTS J1:V & J2:H 34
FIGURE 7-5 : COPOLAR COMPONENT COMPARISON FOR INDIVIDUAL ELEMENTS, LEFT) VERTICAL POLARIZATION (J1) AND RIGHT) HORIZONTAL POLARIZATION (J2) 36
FIGURE 7-6 : CROSSPOLAR COMPONENT COMPARISON FOR INDIVIDUAL ELEMENTS, LEFT) VERTICAL POLARIZATION (J1) AND RIGHT) HORIZONTAL POLARIZATION (J2) 37
FIGURE 7-7 : DEVIATION MASK IN AMPLITUDE FOR (LEFT) HORIZONTAL POLARIZATION AND (RIGHT) VERTICAL POLARIZATION 38
FIGURE 7-8 : DEVIATION MASK IN PHASE FOR (LEFT) HORIZONTAL POLARIZATION AND (RIGHT) VERTICAL POLARIZATION 39

FIGURE 7-9 : COMBINED H & V (POLARIMETRIC) DEVIATION MASK FOR HORIZONTAL AND VERTICAL POLARIZATION THETA RANGE ±30° (LEFT) FOR AMPLITUDE AND (RIGH) PHASE..... 40
FIGURE 7-10: RESULTS OF GAIN MEASUREMENT INVESTIGATION AND ANTENNA LOSS 41
FIGURE 7-11 ANTENNA ELEMENT INSIDE THE THERMAL CHAMBER COVERED WITH ABSORBERS 42
FIGURE 7-12: REFLECTION AND ISOLATION BETWEEN PORTS VS TEMPERATURE (SN47)..... 42
FIGURE 7-13 PHOTOGRAPHS OF THE FACE-TO-FACE SETUP ASSEMBLY. THE METALLIC HOUSING IS INTERNALLY COVERED WITH ECCOSORB SF ABSORBER..... 43
FIGURE 7-14: VARIATION OF TRANSMISSION PARAMETERS VS TEMPERATURE AND FREQUENCY IN FACE-TO-FACE TEST 44
FIGURE 7-15 DEFINITION OF TRIHEX-SMOS RADIATING SUBSYSTEM WITH RADIATING ELEMENTS USED IN THE BB OF THE ANTENNA INSTRUMENT 45
FIGURE 7-16 THERMAL CHAMBER PHOTOGRAPH FOR T7 TEST..... 45
FIGURE 7-17: MEASURED COUPLING TERMS FOR SN04 AND SN08 (T=−10ºC TO +40ºC) 47
FIGURE 7-18 PHOTOGRAPH OF ALBA COMPLETE BREADBOARD AT DTU TEST CHAMBER. 51
FIGURE 7-19 ELEMENTS ORIENTATIONS AND LOCAL COORDINATE SYSTEMS 51
FIGURE 7-20 : COPOLAR RADIATION PATTERN FOR THE COMPLETE SET OF BREADBOARD ANTENNAS 53
FIGURE 7-21 : CROSSPOLAR RADIATION PATTERN FOR THE COMPLETE SET OF BREADBOARD ANTENNAS 54
FIGURE 7-22 : DEVIATION MASK IN AMPLITUDE FOR (LEFT) HORIZONTAL POLARIZATION AND (RIGHT) VERTICAL POLARIZATION 55
FIGURE 7-23 : DEVIATION MASK IN PHASE FOR (LEFT) HORIZONTAL POLARIZATION AND (RIGHT) VERTICAL POLARIZATION 56
FIGURE 7-24 : COMBINED H & V (POLARIMETRIC) DEVIATION MASK FOR HORIZONTAL AND VERTICAL POLARIZATION THETA RANGE ±30 (LEFT) IN AMPLITUDE AND (RIGHT) IN PHASE 57
FIGURE 7-25: BREADBOARD EFFICIENCY VALUES MEASURED AT DTU FOR: LEFT) VERTICAL POLARIZATION AND RIGHT) FOR HORIZONTAL POLARIZATION 58
FIGURE 7-26: ELEMENTS POSITIONS AND PEAK DIRECTIVITIES IN THE BREADBOARD CONFIGURATION..... 59
FIGURE 8-1: TRIHEX INSTRUMENT TOPOLOGY (MARTIN-NEIRA ET AL, 2023)..... 60
FIGURE 8-2: HEXAGON POPULATION AND ROTATION OF SIMULATED (LEFT) AND MEASURED (RIGHT) ANTENNA PATTERNS 61
FIGURE 8-3: RECOVERED MIXED-SCENE (LEFT), OCEAN + RFI SCENE (CENTRE) AND IMPULSE RESPONSE CUT (RIGHT) 61
FIGURE 8-4: FLOOR ERROR OF MEASURED PATTERNS FOR A SINGLE HEXAGON (LEFT) AND THE ONES OF TRIHEX (RIGHT), FOR H AND V POLARIZATIONS 62
FIGURE 8-5: RECONSTRUCTION ERROR AFTER APPLYING SMALL ERRORS TO THE ANTENNA PATTERNS..... 63

TABLES

TABLE 5-1 ALBA ANTENNA MASS BUDGET 20
TABLE 6-1: RESULTS FOR EACH ELEMENT AND POLARIZATION IN THE ARRAY: DIRECTIVITY, CROSSPOLAR VALUE AND -3DB BEAMWIDTH. 28
TABLE 6-2: RESULTS FOR SINGLE ELEMENT: DIRECTIVITY, CROSSPOLAR VALUE AND -3DB BEAMWIDTH FOR EACH POLARIZARION. 29
TABLE 7-1: ANTENNA PERFORMANCE AT THE CENTRE FREQUENCY (1413.5 MHZ) 35
TABLE 7-2: COMPARISON OF COUPLING TERMS V-V FOR MEASUREMENT/SIMULATION 48
TABLE 7-3: COMPARISON OF COUPLING TERMS H-H FOR MEASUREMENT/SIMULATION 48
TABLE 7-4: COMPARISON OF COUPLING TERMS V-H FOR MEASUREMENT/SIMULATION 49
TABLE 7-5: COMPARISON OF COUPLING TERMS H-V FOR MEASUREMENT/SIMULATION 49
TABLE 7-6: BREADBOARD ARRAY ELEMENTS PERFORMANCES AT CENTRE FREQUENCY (1413.5MHZ) 52
TABLE 8-1 FLOOR ERROR STANDARD DEVIATION 62

1. SCOPE

This Executive Summary Report summarizes the activities developed in the frame of the Advanced L-band Antenna for New Generation SMOS Missions (ALBA) ESA contract. The activities consist on design and analyse as well as manufacture and test the ALBA antenna including the assessment of the effect of mutual couplings between elements when integrated into the array. Moreover, at system level, an image analysis reconstruction study has been performed to analyse the improvement on the image quality reconstruction achieved by reducing the spacing between antennas. Results of the design activity of the ALBA antenna as well as the test campaign conducted are summarized in this document.

This Executive Summary also comprises an excerpt of the simulations and analysis performed for the ALBA antenna elements integrated into the TriHex array structure. The document includes the patterns and mutual coupling results of a portion of the TriHex S/C instrument that comprises a complete side of the structure and several elements of the neighbouring sides. A summary of the test results obtained in the test campaign performed to the ALBA antenna breadboard are included. Instrument performance assessment covering the simulation and image reconstruction analysis have been developed in the frame of ALBA project considering the TriHex mission with 3 spacecrafts in formation flying.

2. APPLICABLE AND REFERENCE DOCUMENTS

2.1 APPLICABLE DOCUMENTS

AD	Doc. No.	Issue/ Rev.	Title
[AD01]	ESA-TEC-SOW-023077	1.1	Statement of Work L-Band Antenna for Next Generation SMOS Missions.
[AD02]	ASE-O-00343-01-0	1.1	Technical Proposal of ALBA - Advanced L-Band Antenna for NG SMOS Missions
[AD03]	ALBA-CCN001_iss01. 136182 CCN 1		CCN1 to ESA contract. 4000136182/21/NL/AS

2.2 REFERENCE DOCUMENTS

RD	Doc. No.	Issue/ Rev.	Title
[RD01]	ALBA-ADSM-TN-1001602782	02	TN4: ALBA: Antenna Detailed Design.
[RD02]	ALBA-ADSM-TN-1001799483	01	TN4 addendum 1: Antenna Design Updates DDR
[RD03]	ALBA-ADSM-TN-1001843223	01	TN4 addendum 2: Array Patterns & coupling simulation
[RD04]	ALBA-ADSM-TN-1001602782	03	TN5: ALBA Test Plan
[RD05]	ALBA-ADSM-TR-1001983557	02	TN6: Antenna Test Report.
[RD06]	ALBA-ADSM-TR-1002011047	01	Annex 1 TN6 Phase Centre
[RD07]	ALBA-TN-UPC-001	01	Image Reconstruction and Instrument Performance",

2.3 ACRONYMS

ABBV	Abbreviation
AD	Applicable Document
ASE	Airbus Defence and Space España
DTU	Technical University of Denmark
ESA	European Space Agency
GP	Ground Plane
RD	Reference Document.
MGSE	Mechanical Ground Support Equipment
RD	Reference Document.
RF	Radio-Frequency.
SMOS	Soil Moisture and Ocean Salinity.
SOW	Statement of Work
SMP	Sub-miniature Push-On
TRB	Test Review Board
UPC	Universitat Politécnica de Catalunya
VNA	Vectorial Network Analyser.

2.4 PAPERS PUBLISHED

1. Garcia-Garcia, Q., Espinosa, D., Zurita, A., Closa, J., Gandini, E., Suess, M., Martin-Neira, M.., "*Antenna Element Study for a Future SMOS Mission*," 2022 16th European Conference on Antennas and Propagation (EuCAP), Madrid, Spain, 2022, pp. 1-5, doi: 10.23919/EuCAP53622.2022.9769389.
2. Garcia-Garcia, Q., Lopez-Yela, A., Zurita, A., Olea, A., Martin-Neira, M., Gandini, E., Suess, M., "*Antenna Design for TriHex: A Future Soil Moisture and Ocean Salinity Radiometer Mission*," 2024 18th European Conference on Antennas and Propagation (EuCAP), Glasgow, United Kingdom, 2024, pp. 1-5, doi: 10.23919/EuCAP60739.2024.10501276.
3. A. Lopez-Yela, Q. Garcia-Garcia, A. Olea, A. Zurita, E. Gandini, M. Martin-Neira, M. Suess, "*TriHex Antenna Design: First Measurement Results* ", 42th ESA Antenna Workshop, November 2024, Noordwijk, the Netherlands
4. Q. Garcia-Garcia, A. Lopez-Yela, A. Olea, A. Zurita, E. Gandini, M. Martin-Neira, M. Suess , I. Corbella, "*TriHex Antenna Design and Performance Assessment Results*", Submitted to ESA Living Planet Symposium 2025
5. I. Corbella, M. Martin-Neira, Q. García, A. Lopez-Yela, A. Olea, A. Zurita and E. Gandini., "*TriHex Imaging Simulation*", SMOS Science Conference, November 2024, Calatabiano, Sicily, Italy

3. INTRODUCTION

Final report of Advanced L-Band antenna for NG SMOS Missions (ALBA) summarizes the activities performed during the program including design, performance review and test results of ALBA antenna isolated element, as well as system simulations performed with simulated and pattern test results to feed the UPC simulator to predict system performances.

During the ALBA project execution, the initial Instrument was updated from one single hexagonal large structure with the elements located at the center of the hexagon segments to a 3 spacecrafts instrument with formation flying called TriHex, in which the antenna elements are located at the edge of each individual spacecrafts structure.

This modification implied a physical and RF update of the ALBA antenna and it was also built a 3D CST model of a portion of the TriHex Instrument to perform the corresponding antenna simulations, and based on this an antenna breadboard composed of 11 radiating elements was designed, manufactured and tested. The modifications from the original structure defined at the ITT to the TriHex instrument implied an impact on the RF antenna performances due to the new location of the antenna elements at the edge of the spacecrafts structure, and therefore it was necessary to adequate the ALBA full antenna breadboard definition and test campaign to the TriHex structure. Aligned with this, the updated TriHex structure and mission with three S/C in free falling formation flying were also considered by UPC to perform the associated system simulations.

This report comprises all simulations and analysis performed for the ALBA antenna elements integrated into the TriHex array structure. CST Studio Suite is the tool used for the antenna analysis both individual and in arrayed configuration (a 3D CST model has been built to simulate a portion of the TriHex Instrument). Comparisons between RF test results and simulation as well as the requirements review have been also included in this final report.

Finally the Instrument performed assessment performed by UPC in the frame of ALBA considered the simulation and image reconstruction analysis of the TriHex with 3 spacecrafts in free-falling formation flying.

4. BACKGROUND OF THE PROJECT

SMOS has been in orbit since 2009, Soil Moisture and Ocean Salinity mission is based on a n L-band interferometric radiometer providing images of the entire earth globe every three days, which has allowed to learn significantly on the reconstruction process of the synthetic aperture radiometer and the influence of the correspondent calibration parameters.

Several studies conducted during last years have concluded that the most promising solution to improve the image quality reducing the imaging time is based on an hexagonal array with inter-element distance of 0.767λ. The improvement can be even higher by designing an alias-free array solution by reducing the inter-element distance to 0.577 λ (at 1413.5 MHz). In this way the revisit period can be reduced by a factor 3 compared to the MIRAS instrument and the image quality is expected to improve.

This is the origin of ALBA project, which objective is to design, manufacture and demonstrate through tests, the performances of a representative part of an hexagonal L-band array antenna with reduced element spacing of 0.577λ to enlarge the alias-free region.

For this purpose a patch antenna has been designed and selected as baseline for ALBA. Each antenna element is a single individual that operates in dual polarization in the RF band designed for the instrument (1404MHz-1423MHz).

ALBA antenna consists of a circular disk with a central metallic supporting post surrounded by a cylindrical cavity. The patch antenna is fed at four points with a balanced feed network to provide crosspolar cancellation and high isolation between the V and H ports.

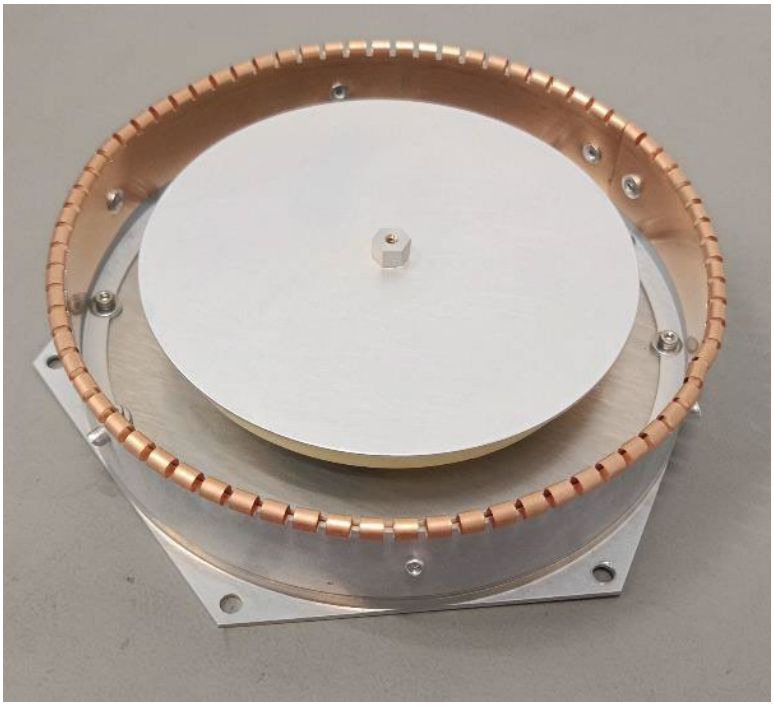

Figure 4-1: photograph of assembled antenna model

The design of the balanced feed network is based on the former design of circuit designed for the SMOS-MIRAS antenna with a number of modifications that have been considered to adapt the design to the current geometry and also to improve the performances with respect the previous design. In this line Duroid 6002 from Rogers instead Teflon as in SMOS antenna has been selected as substrate for ALBA antenna.

In ALBA project an engineering model including 11 elements has been built to test the concept. After updating the mission to TriHex (Figure 4-2), the initial definition of the engineering model was adapted to TriHex configuration (Figure 4-3).

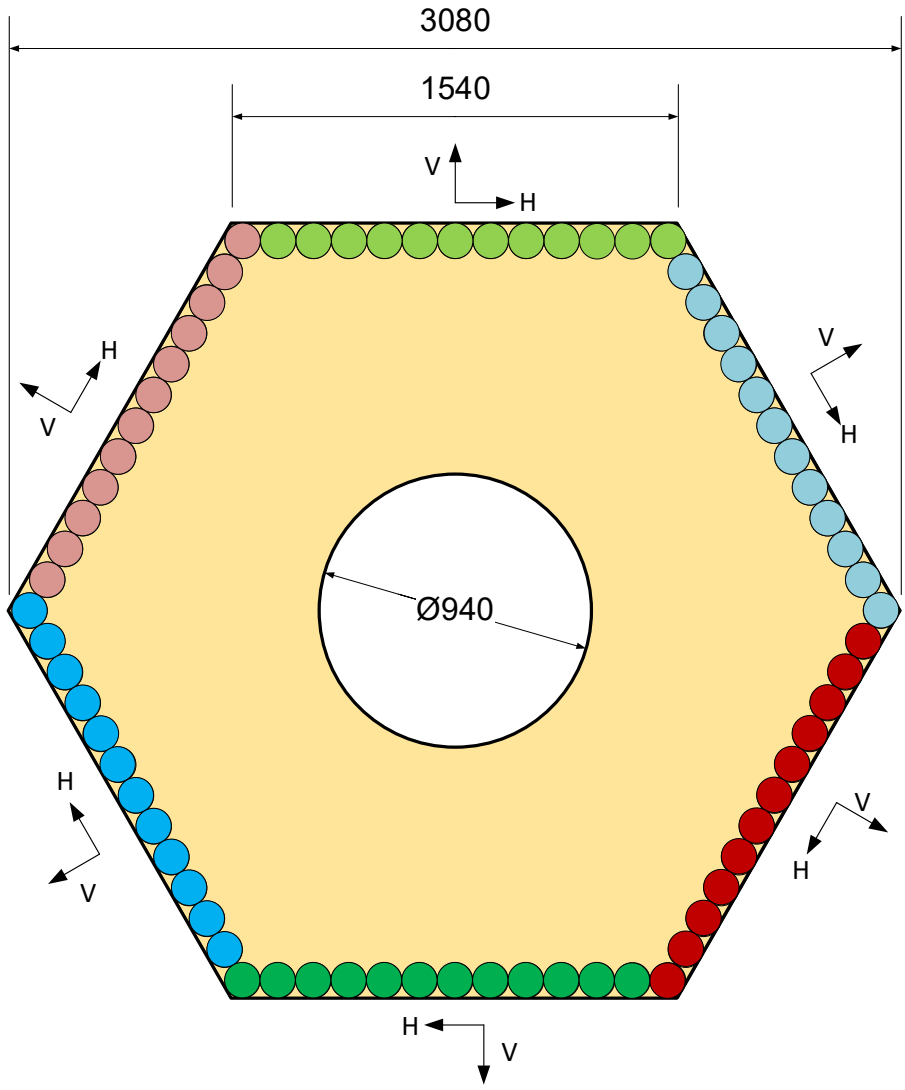

Figure 4-2: definition of TriHex-SMOS radiating subsystem with radiating elements used in the BB of the antenna Instrument

The ALBA/TriHex breadboard is composed by the 11 antenna elements arranged in the perimeter of the structure with the distribution of the polarization ports as shown in **Figure 4-3**.

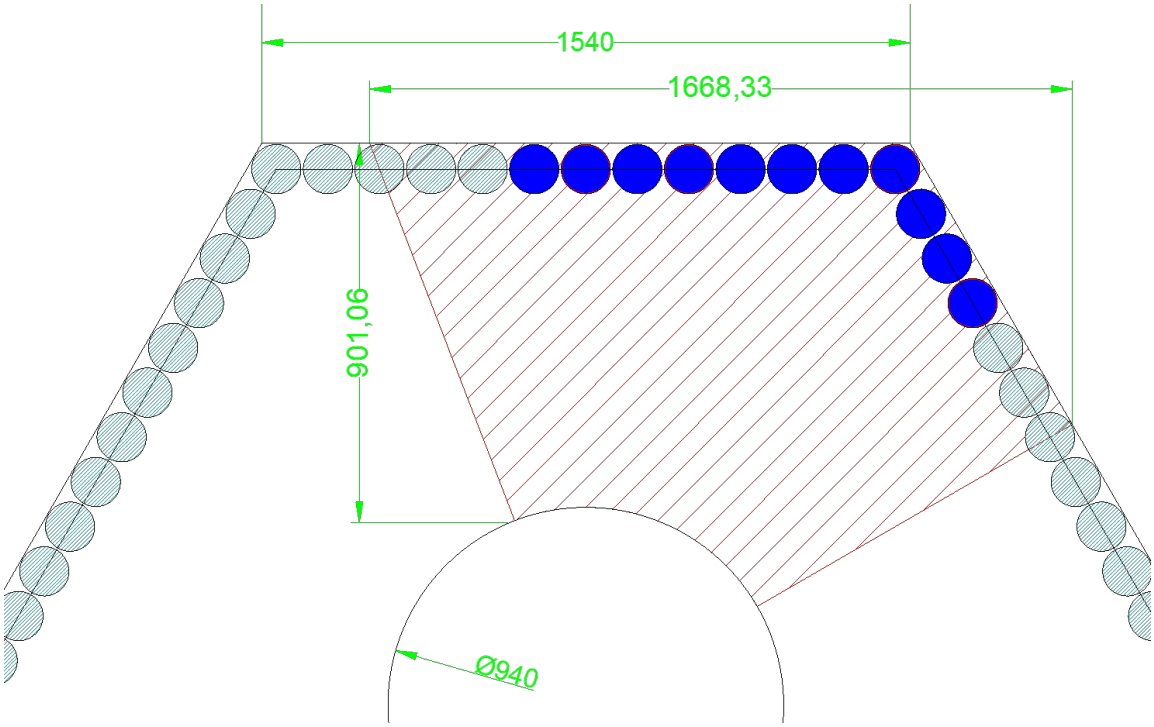

Figure 4-3: Definition of ALBA-TriHex breadboard.

S-parameters and mutual coupling, both in ambient and temperature, have been tested. Also, the radiation patterns measurements of the breadboard portion of the TriHex S/C instrument have been done. All this information will be summarized along the document.

Finally by using the radiation patterns simulated and measured of the ALBA antenna elements on the breadboard, and by means of an image reconstruction simulator developed by UPC, a hexagonal instrument configuration is also analysed in TriHex configuration, so, with 3 s/c instrument in formation flying .

5. ALBA ANTENNA

5.1 RADIATING ELEMENT DESCRIPCION

The antenna is a disk patch antenna fed with four capacitive probes located at 90º one of the other. The four probes are connected to a printed circuit at a lower level. This printed circuit is made in microstrip technology and the circuit layout guarantees that the signals arrive with the correct phases to the feed points. The circuit PCB contains two independent circuits that allow the connection of each pair of probes with the correct 180º phase, and one independent input connector is associated to each of these subcircuits.

The antenna concept, which is mostly metallic, has fed from the developments that have been performed lately for the Galileo antennas with metallic elements and cavities. This is a difference with respect the design of the initial MIRAS-SMOS antenna.

The external size of the antenna is approximately 114mm in diameter including the external part, and has a height of 25mm approximately. Attending the RF concept of the antenna, the radiating part (the patch antenna) is situated inside a metallic cylindrical cavity, and the feed probes as well. The circuit is contained in a metallic housing with hollow guides that follow the PCB traces but not in contact with them except in the required areas. This form a kind of sandwich with the metal housing and the central PCB.

In Figure 5-1 it is shown the section of the cavity in which the patch antenna is located. The patch antenna is modelled as a patch disk element. The surrounding cavity is made in aluminium as the patch itself.

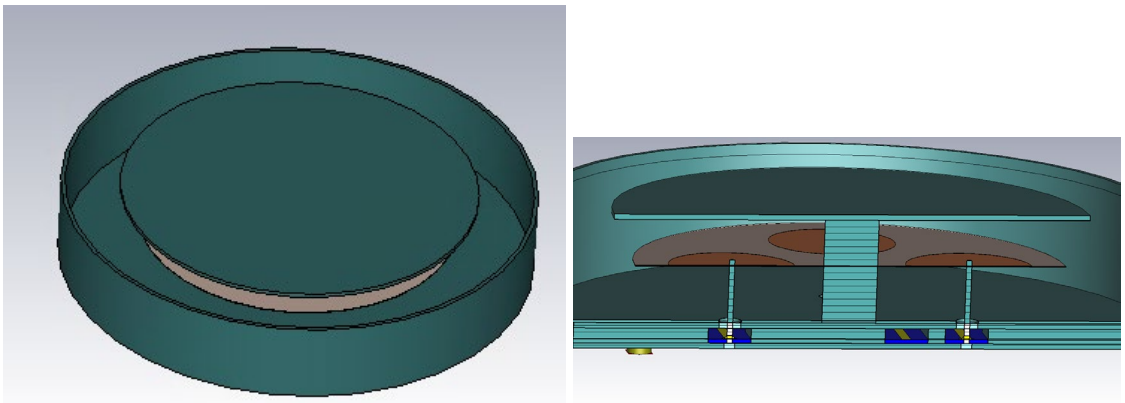

Figure 5-1: 3D views of the antenna cavity

The central cylindrical piece is made also in aluminium and guarantees the correct height of the patch antenna with respect the ground plane. It includes a piece screwed to the lower part (the PCB spacer) and also screwed from above to the patch antenna.

The feeding PCB is located below the antenna cavity, at a lower level from those shown above. It is separated from the antenna cavity with a ground plane.

In Figure 5-2 is shown the PCB and the feed network layout traces. The connections that can be seen at the left of the figure are the connections to the input connectors that are located at a lower level of the antenna.

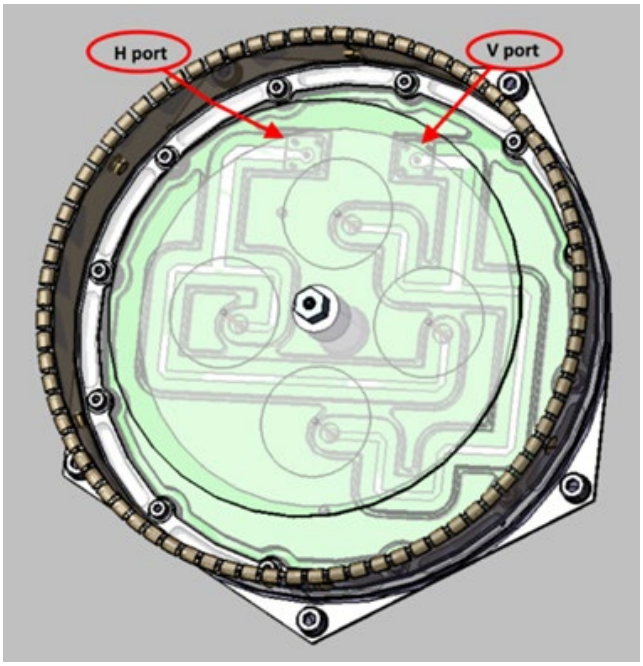

Figure 5-2: 3D view of the feed network for the antenna

In the current design no dielectric spacer has been considered for the feeding pins of the antenna as requested by ESA. The feeding pins are directly soldered to the balanced feed network on one side and to the capacitive feed network on the other, as in **¡Error! No se encuentra el origen de la referencia.**.

The central screw is a custom design that allows the installation of the optical jig necessary for the alignment of the antenna in the setup.

In Figure 5-3, the hexagonal footprint of the antenna is shown, with a width of 114mm compatible with the spacing between elements specified (0.577λ=122.5mm).

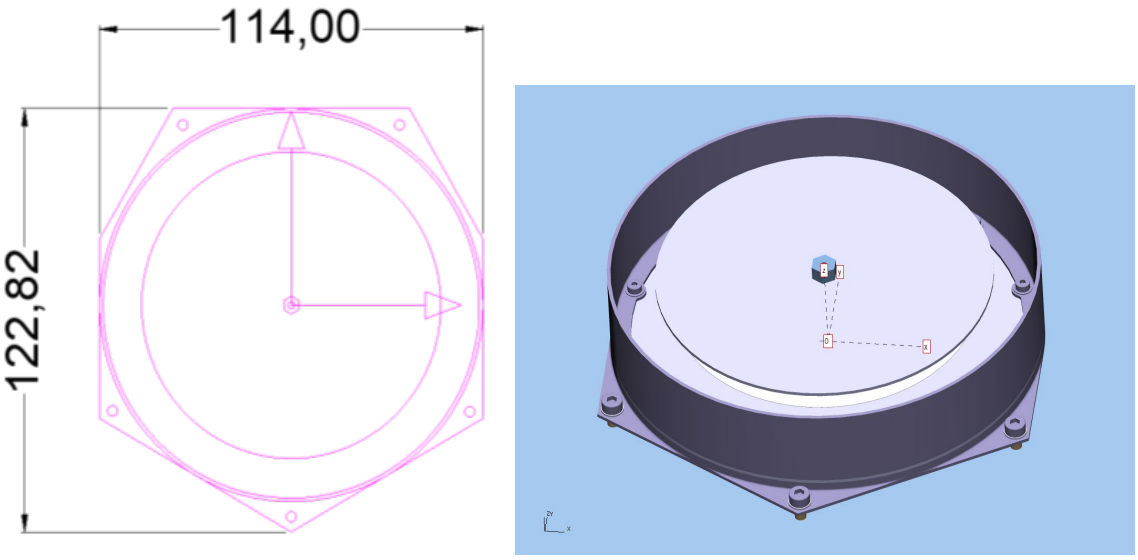

Figure 5-3: geometry of the antenna structure for integration in the hexagonal TriHex instrument

Finally, Figure 5-4 shows a 3D cross section of the antenna which shows the division of the central supporting element to hold the feeding PCB assembly as well as other parts of the internal elements of the antenna (feeding pins, feed network PCB, metallic housing, etc…)

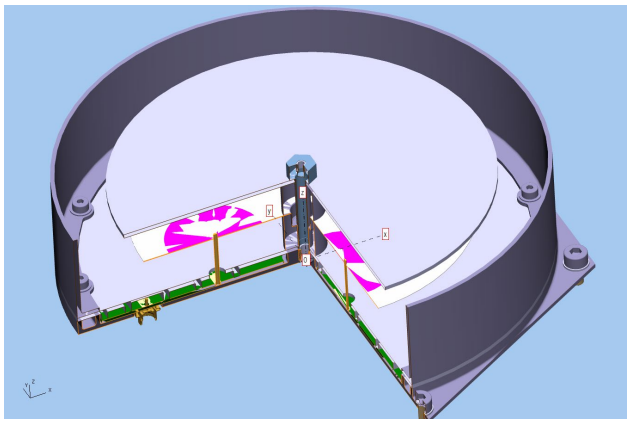

Figure 5-4: 3D Cross-section of the SMOS ALBA antenna

The antenna will be mounted on a structure surrounding the circular cavity, and in order to avoid possible leakage radiation of the gap between antenna and the surrounding cavity and ground plane, it is necessary to guarantee the conduction between the cavity and the structure, which was achieved with a fingerstock metallic gasket. The gasket part is COTS, manufactured by Leader Tech and it allows closing the gap as sketched in Figure 5-5.

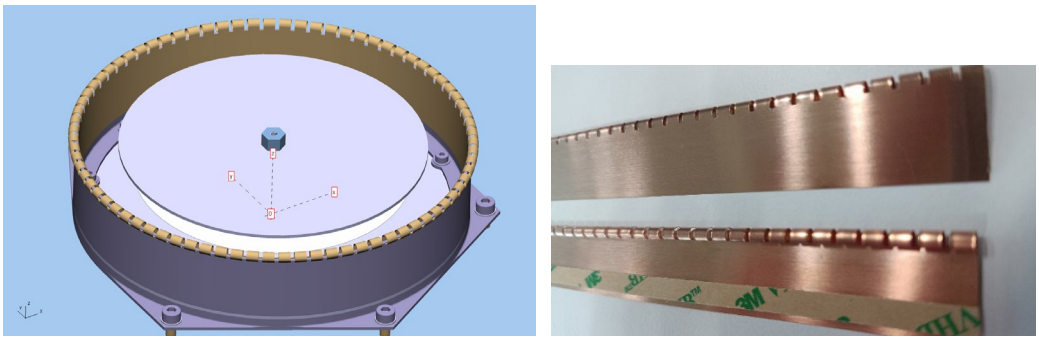

Figure 5-5 ALBA antenna element with closing gasket (provided by Leader Tech)

mass budget

Total antenna mass including the 5 attachment screws is 154g (Table 5-1).

Bill of Material: ALB00AE0000				
Part Number	Name	Unit Mass (kg)	Quantity	Mass (g)
ALB00AE0001	BASE	40	1	40
FEEDING PCB	FEEDING PCB	13	1	13
ALB00AE0002	GROUND PLANE	37	1	37
ALB00AE0003	CAVITY	24	1	24
ALB00AE0004	CENTRAL SPACER 01	2	1	2
CAPACITIVE PROBES	CAPACITIVE PROBES	1	1	1
ALB00AE0008	EXCITATION PIN	0,1	4	0,4
ALB00AE0005	CENTRAL SPACER 02	2	1	2
ALB00AE0006	PATCH ANTENNA	17	1	17
ALB00AE0007	CENTRAL SCREW	0,8	1	0,8
SMP: 19S102-400L5	STRAIGHT PLUG	0,5	2	1
ISO_4762-M2x6-A4.70	SCREW	0,4	12	4,8
ISO7089-2-200HV-A4	WASHER	0,04	12	0,48
ISO_4762-M3x6-A4.70	SCREW	0,04	5	2
LN9016-03M	WASHER	0,08	5	0,4
12-75RS-XX-16 REV B1	GASKET	8	1	8

Table 5-1 ALBA antenna mass budget

5.2 TRIHEX SPACECRAFT INSTRUMENT CONFIGURATION

During the project, ESA informed that the instrument configuration had been modified, and the new geometry indicated in Figure 5-6 was applicable, with the elements included per side. In the current TriHex configuration the element spacing is kept in 0.577λ as in the original configuration, but the overall antenna size is reduced which also reduces the

synthetic antenna beamwidth/resolution. Each side of the hexagonal configuration of the instrument is now populated with 13 elements, 12 with the same polarization and 1 with the tilted polarization of the next segment, and the more relevant change from the antenna element design point of view is the location of the antenna elements at the edge of the instrument top plane structure which is assumed conductive.

The number of antenna elements included in the instrument is $12 \times 6 = 72$ units.

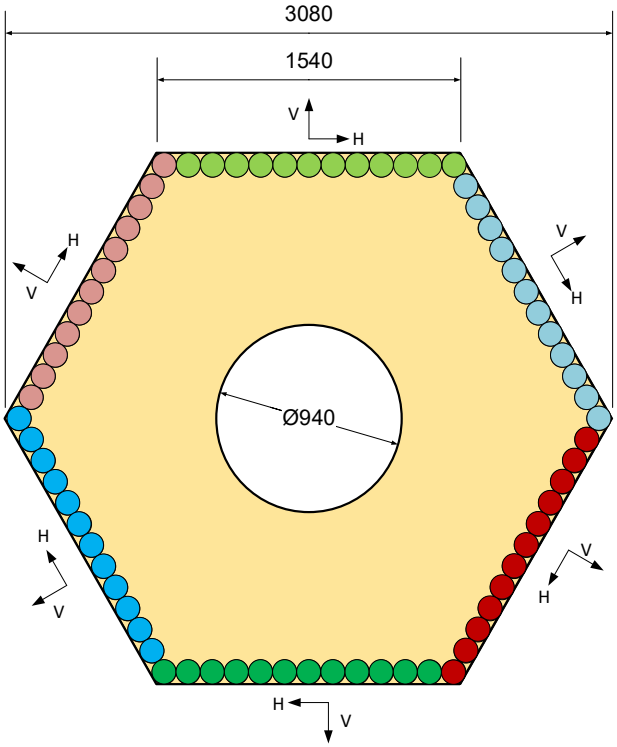

Figure 5-6 relative orientations of the radiating elements in the radiating aperture of TriHex. Each colour indicates a different polarization orientation respect a common view point.

For the orientation, all the radiating elements have the same relative orientation with respect their side, which implies that the orientation of the antennas with respect a common polarization axis makes a full rotation in steps of 60º: 0º, 60º, 120º, 180º, 240º, 300º. This is illustrated in Figure 5-6,associating a color code to each orientation.

The new configuration of the instrument led to an analysis of the impact of the new arrangement on the mutual coupling between elements and the impact on the radiation pattern, presented during the PM3.

6. SIMULATION RESULTS

6.1 INDIVIDUAL ANTENNA ANALYSIS

The single antenna was studied under different scenarios such as isolated with no ground plane, at the center of a squared ground plane or at the edge of the ground plane (a size of 90x90cm was considered as per the ITT requirement). Also, a tolerance analysis was performed at simulation level to certify the design robustness (RD1,RD2,RD3 for completeness). CST was used as a 3D EM tool for the analysis.

It was also agreed to locate the antenna at the edge of the 90x90cm ground plane, to be more representative of their position in the S/C, and both analysis and testing of the individual performances of each element were made in this configuration.

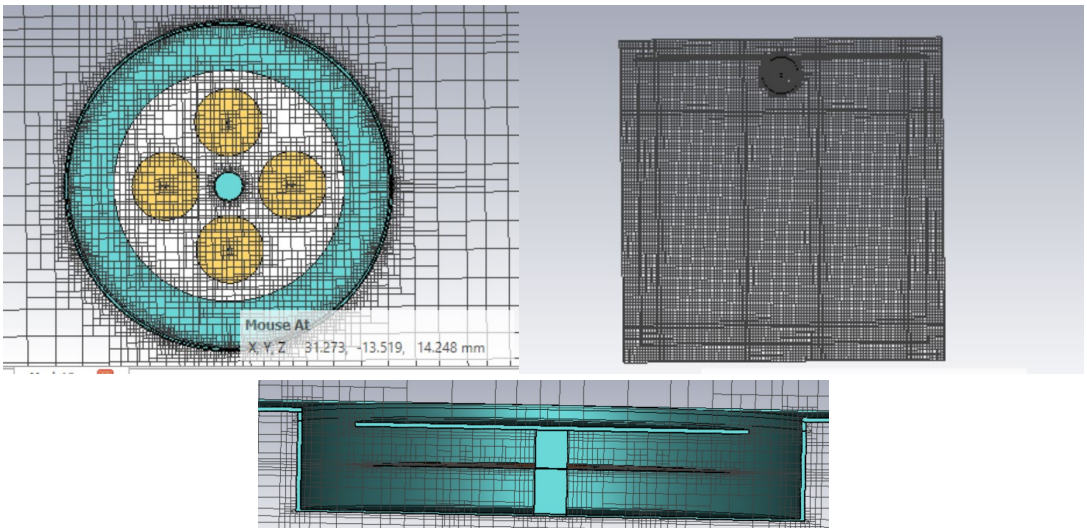

Figure 6-1: Antenna meshing for simulation in CST

S-parameters and radiation patterns results are included as baseline for measurement comparison.

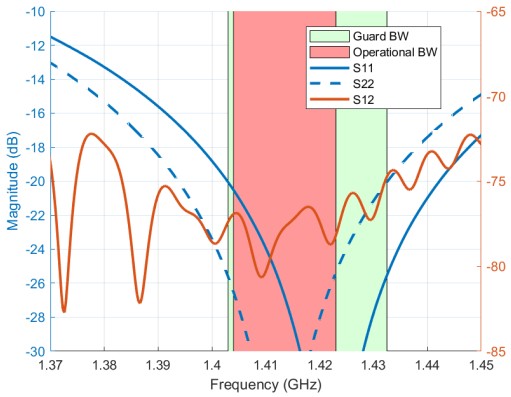

Figure 6-2: S-parameter performance in simulation for the individual antenna at the edge of the ground plane.

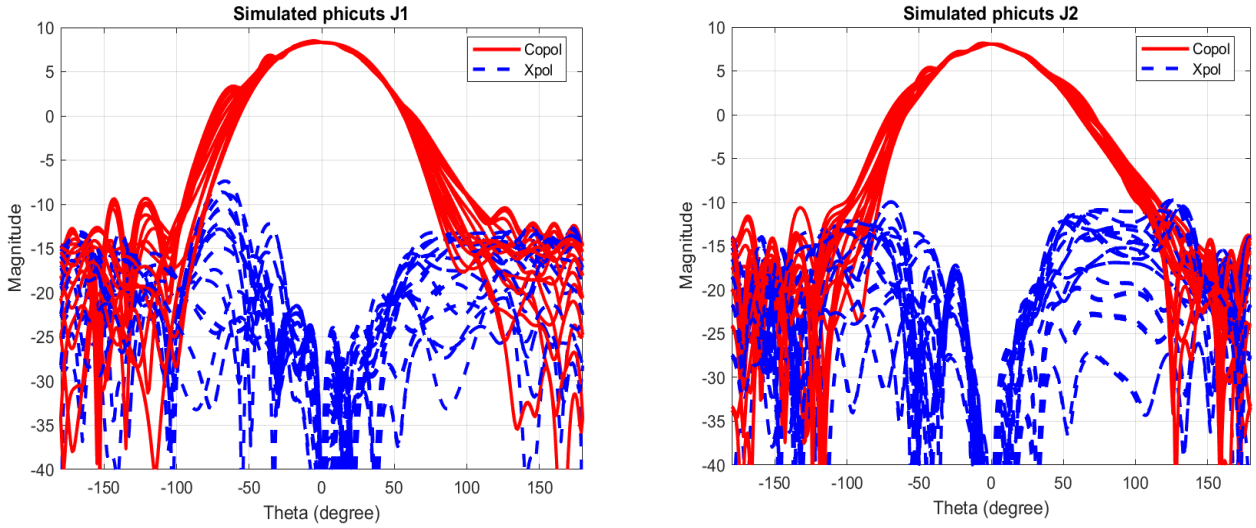

Figure 6-3:Radiation pattern simulated performances at the centre frequency, left) vertical polarizacion and right) horizontal polarization.

The effect of the antenna position on the ground plane produces a variation in the current distribution in the antenna surroundings, varying both S-parameters and radiation pattern. This effect was also studied during the project.

Concerning the radiation pattern, when the antenna is moved to the edge, a non-symmetrical diagram is obtained, as a result of the modified current distribution around the element, and this produces a crosspolar level increase with respect a centred arrangement, due to the fact that cancelation along the axis parallel to the edge (X-axis) is not complete as the current strength at these edges of the antenna are not of the same magnitude. Also, the copolar component is affected with ripple as it is illustrated in Figure 6-3.

6.2 TRIHEX ARRAYED ANTENNA ANALYSIS

Running an electromagnetic simulation with CST of the complete TriHex spacecraft should have been a formidable task in terms of memory and computer resources required by the model. Therefore the solution adopted was to define a subsection of the spacecraft which could be considered electromagnetically representative. In antenna problems this usually implies the definition of the number of ‘active elements’, the number of ‘dummy’ elements and the representative surrounding structure, and the resulting size of the electromagnetic problem must be compatible with the computer capabilities (memory and resources). Due the symmetry of the TriHex structure, the configuration that was studied was a section of the structure corresponding to 1/6 of the complete model. It was analysed in terms of computer resources and it was found compatible (although simulation time was very large).

In this case, from the 19 antenna elements included in the model there are 4 dummies (E15, E16, E18 and E19) located at the edges which produce the coupling level necessary to make the others be representative, and therefore the other 15 are considered representative of the real physical model. This configuration permits to characterize, as accurate as possible,

corner elements and mitigate the ground plane truncation. A complete full wave simulation was performed to extract radiation pattern and mutual coupling information of the complete side (from E1 to E13) including the metallic walls (both frontal and lateral) present in the design of the structure.

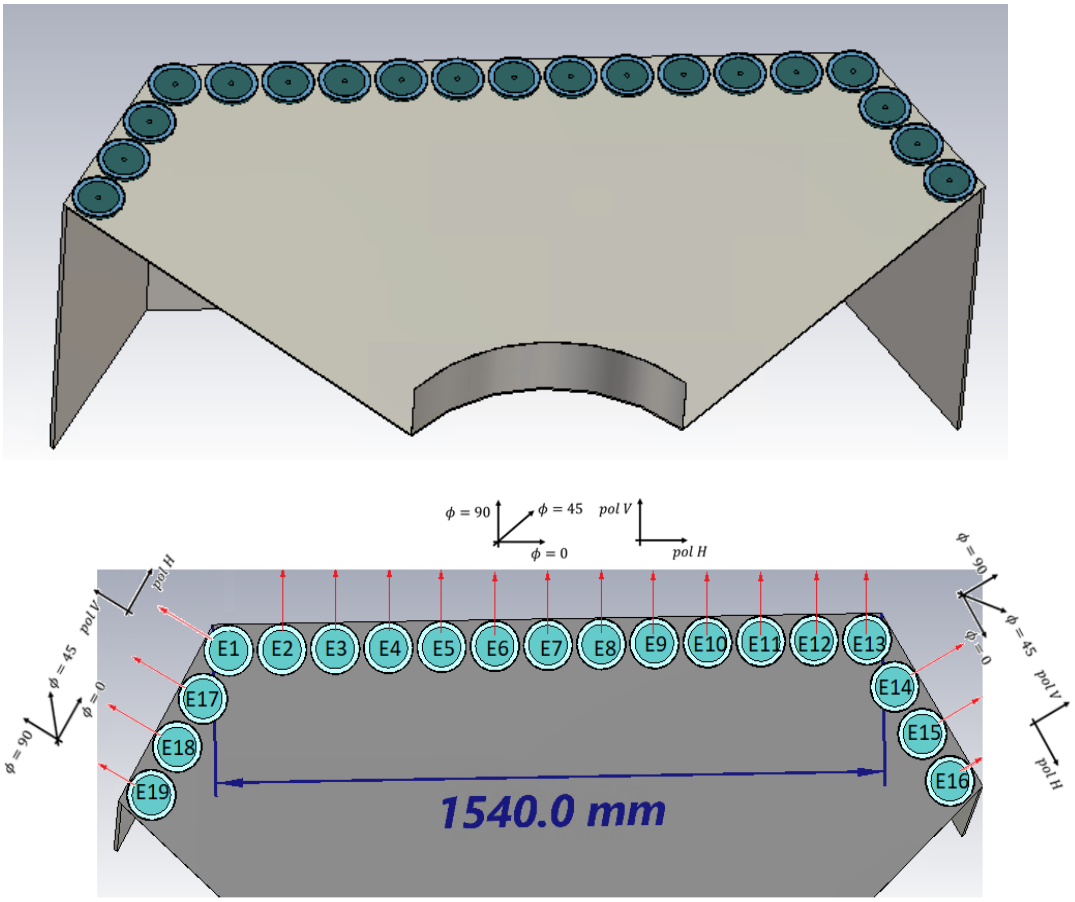

Figure 6-4:·3D EM model to characterize the TriHex configuration

The red arrow illustrates the vertical polarization of each element. The horizontal polarization is defined parallel to each side edge. The elements E14-E19 at the left and right sides are rotated +60 and -60 degrees with respect the central elements that are the objective of the analysis (E1-E13). The radiation pattern for each element has been calculated using a local coordinate system for each element. Therefore all the patterns calculated in the model can be compared directly.

Concerning the coupling, next figures show the simulated values for the central element in the arrayed TriHex structure (E7) in V-V, H-H, V-H and H-V polarizations, with respect to different neighbours. A summary of the results is shown here, while RD3 comprises the complete study.

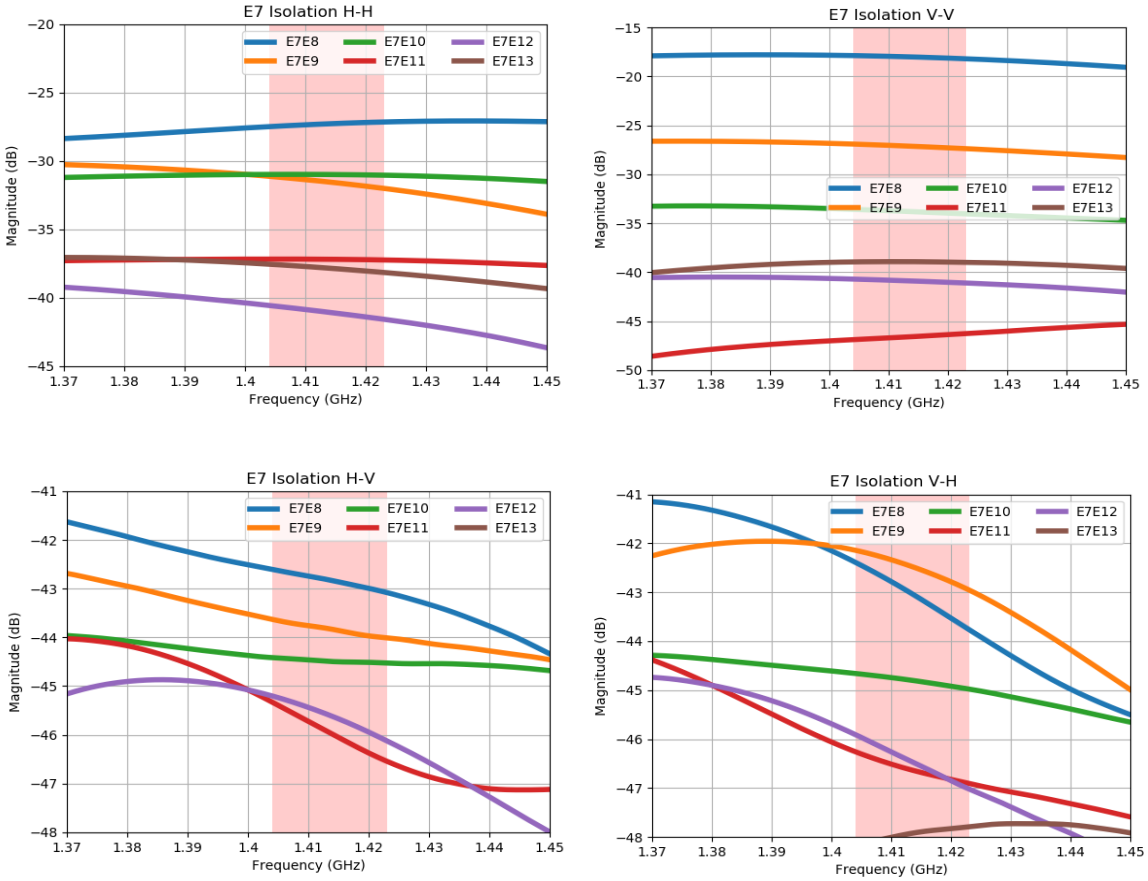

Figure 6-5: Coupling terms (H-H, V-V, H-V and V-H) for the central element of the arm (E7).

In summary, coupling terms in the order of 18dB for VV and about 28dB for HH between closer elements, growing with the separation, but in general with high coupling values due to the close distance between elements, which was expected to produce a noticeable effect at antenna pattern level (both in shape, and gain level). Apart from the coupling, the position of the antenna close to the edge of the TriHex structure should also contribute to modify the isolated antenna pattern.

Figure 6-6 and Figure 6-7 show the radiation pattern for V and H polarization ports for elements E1 to E13, comparing copolar and crosspolar components (without any normalization in its magnitude). Copolar and Crosspolar are calculated by the simulation software according Ludwig 3rd definition of polarization. The copolar versus crosspolar ratio is in line with 20dB from -30 to 30 degrees in theta angle for all the element in the array. It is noticed the effect of the antenna element position in the spacecraft, close to the edge, and also the effect of couplings between neighbouring elements that produces a relevant change in the crosspolar level with respect the individual antenna pattern reported in RD1 and RD3.

Also, the copolar component shows a ripple (already detected in previous studies in the project RD1) produced by the location of the element at the edge of the ground plane. Finally, the on axis crosspolar level of E7 (central element) is lower than the rest of components,

below -60dB, due to cancelations in a symmetric structure with and odd number of elements for phi 90 degrees.

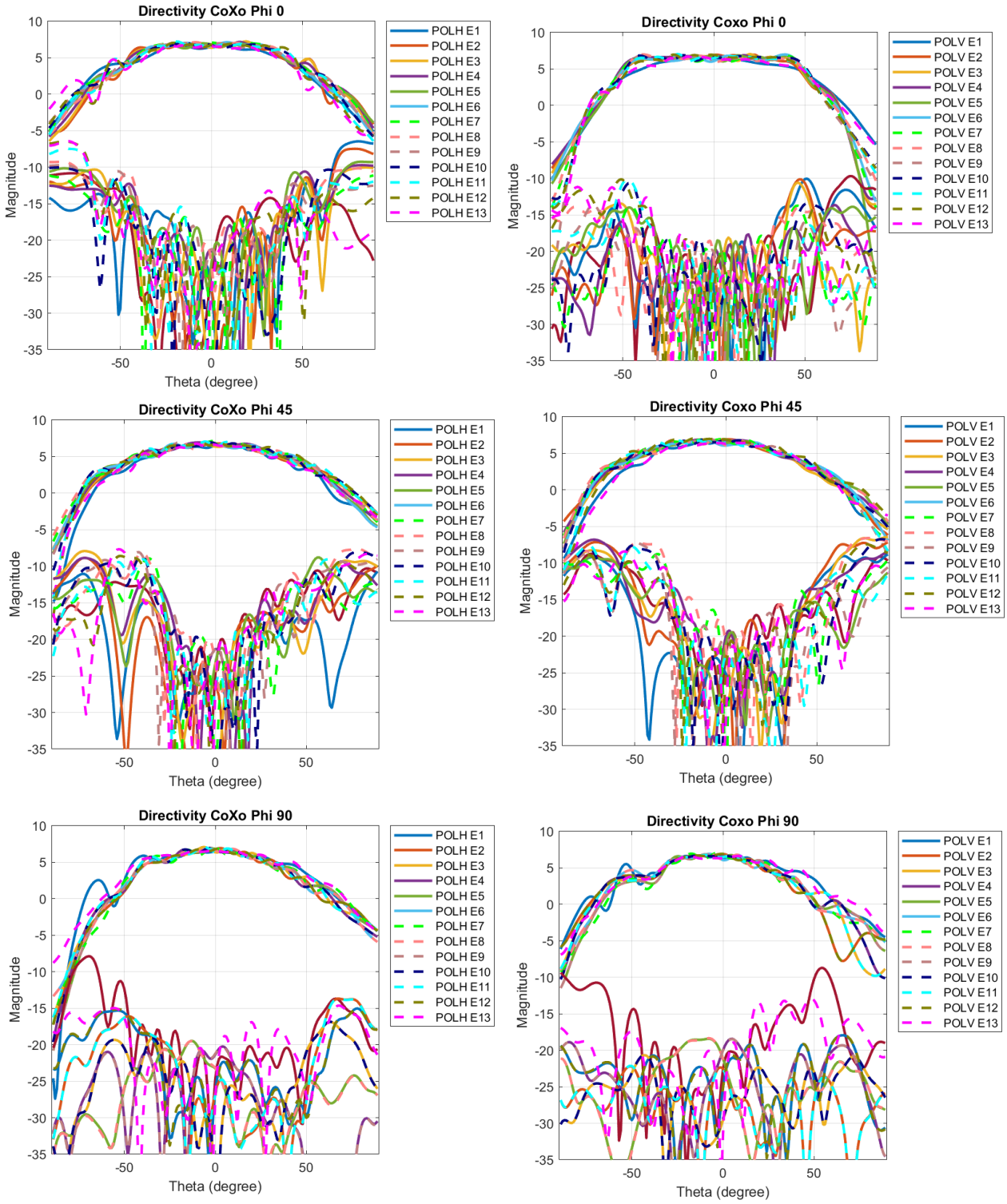

Figure 6-6:Copolar and crosspolar component for elements E1-E13 at phi 0,45 and 90 degrees, left)for horizontal polarization and right) for vertical polarization.

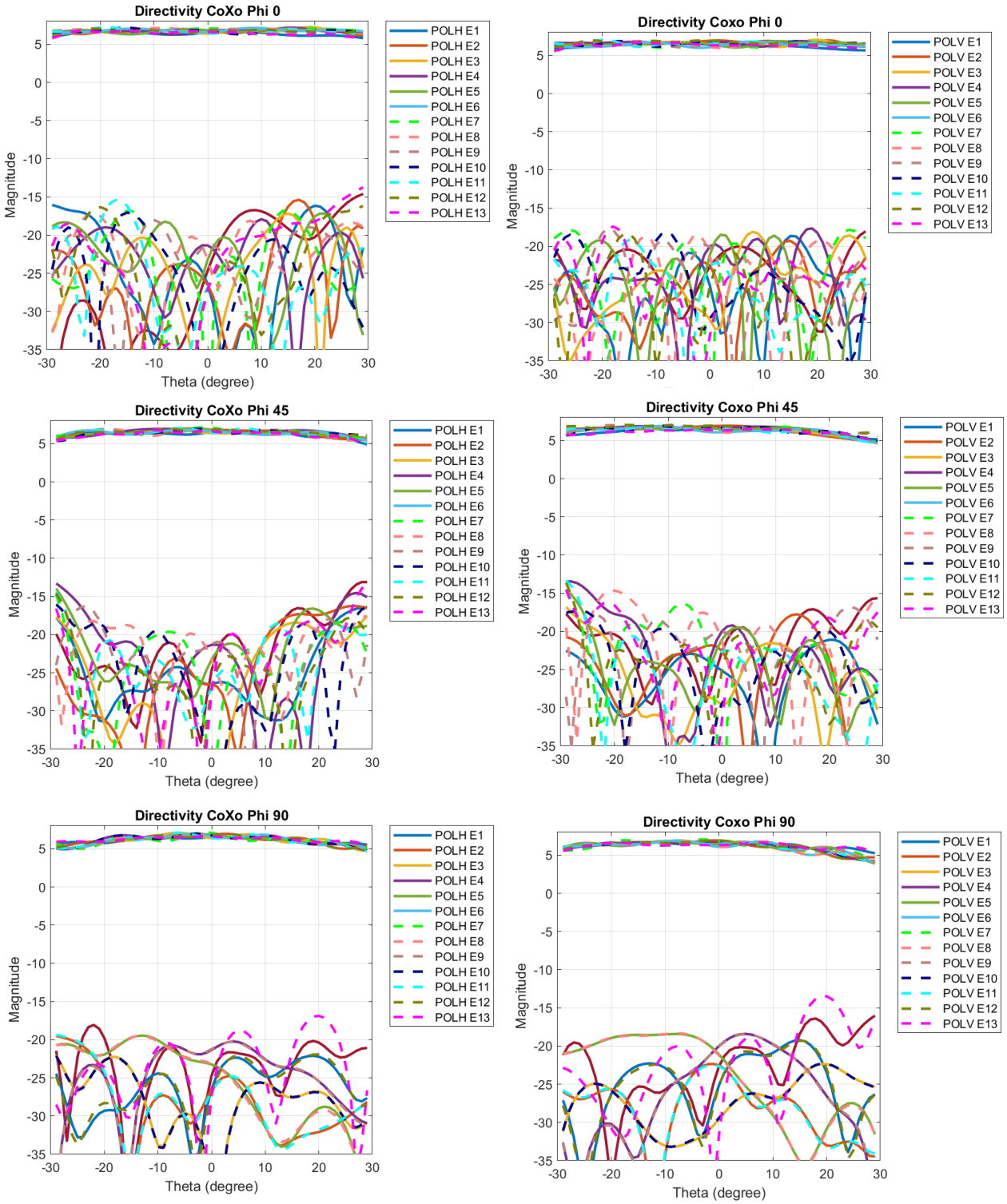

Figure 6-7: Copolar and crosspolar component for elements E1-E13 at phi 0,45 and 90 degrees

Table 6-1 and Table 6-2 show numerical results of the embedded elements and their positions in the TriHex antenna model compared to the individual results. One main effect is

the beamwidth, that is directly related to the loss of directivity; the effect on the shape of the pattern is an effect of the position of the elements close to the ground plane edge, as well as the deformation effect caused by coupling terms excitations between neighbour elements.

For the insertion loss (efficiency) it can be observed that for the individual element (Table 6-2), the loss is in line with the expected values and also with the insertion loss simulated and reported in RD2, with 0.1dB loss for the SMP connector already considered.

In the arrayed results, the insertion loss of the H pol elements is in line with the simulations, but the V-pol port shows a 0.1dB loss increase which it is attributed to the high coupling in VV, that is in the range of -18dB compared to the HH coupling, in the range of -27dB. This coupling value causes a power loss in the V pol of 0.07dB to each of the 2 neighbours located at each side, and this causes a loss increase of ~0.14dB for the V pol with respect the H ports.

	Element number												
parameter	1	2	3	4	5	6	7	8	9	10	11	12	13
Directivity polH (dB)	6.94	7.15	7.39	7.24	7.16	7.23	7.38	7.23	7.16	7.24	7.39	7.15	6.77
GAIN IEEE polH (dB)	6.74	7.00	7.25	7.09	7.01	7.08	7.23	7.08	7.00	7.09	7.25	6.99	6.57
Realized Gain polH (dB)	6.71	6.96	7.20	7.04	6.97	7.04	7.19	7.04	6.97	7.04	7.20	6.96	6.53
HPBW polH phi 0 (deg)	96	92	91	91	97	95	95	95	97	91	90	92	87
HPBW polH phi 90 (deg)	96	76	80	82	83	82	72	82	83	82	80	76	95
XPD polH phi45 (dB) (1)	19.3	21.6	21.3	21.8	18.2	18.7	20.1	21.7	21.8	20.7	19.8	18.7	18.6
Directivity polV (dB)	6.84	7.12	7.15	7.08	7.09	7.15	7.17	7.15	7.09	7.08	7.15	7.13	6.79
GAIN IEEE polV (dB)	6.61	6.84	6.87	6.81	6.81	6.87	6.87	6.86	6.81	6.81	6.88	6.84	6.56
Realized Gain polV (dB)	6.59	6.81	6.84	6.77	6.78	6.84	6.86	6.84	6.78	6.77	6.85	6.81	6.53
HPBW polV phi 0 (deg)	105	100	102	104	102	103	105	103	102	104	101	100	101
HPBW polV phi 90 (deg)	92	68	72	72	64	66	64	66	64	72	71	67	86
XPD polV phi 45 (dB) [1]	21.9	26.9	24.4	24.7	20.6	22.4	29.9	20.5	22	24	21.6	21.8	22.4
Losses PolH (dB)	0.20	0.15	0.15	0.15	0.15	0.15	0.15	0.15	0.15	0.15	0.15	0.15	0.20
Losses PolV (dB)	0.23	0.28	0.28	0.28	0.28	0.28	0.28	0.28	0.28	0.28	0.28	0.28	0.23

(1) For the angular range -30< θ<30

Table 6-1: Results for each element and polarization in the array: directivity, crosspolar value and -3dB beamwidth.

parameter	Isolated	Edge GP (90cm)
Dir polH (dB)	7.7	7.84
Dir polV (dB)	7.7	8.33
XPD polH phi 45 (deg) ([1])	33	22.3
XPD polV phi 45 (deg) ([1])	33	26
HPBW phi 0 polH	76	74
HPBW phi 90 polH	84	72
HPBW phi 0 polV	84	72
HPBW phi 90 polV	76	78
Losses PolH (dB)	0.15	0.16
Losses PolV (dB)	0.18	0.19

Table 6-2: Results for single element: directivity, crosspolar value and -3dB beamwidth for each polarizarion.

In conclusion, from the simulation point of view, a complete analysis of the design antenna has been performed for both single element and the TRIHEX array model, including mutual couplings and their effect on the embedded patterns, and also including a large ground plane representative of the TriHex structure as it was discussed during the DDR. Even-Odd symmetries of the radiation patterns of the elements have been highlighted as they were already noticed in RD1. The spreading effect of the element patterns due to the location of the antenna elements on the TriHex structure has been evidenced.

7. ALBA ANTENNA ELEMENTS TEST CAMPAIGN RESULTS

The test campaign on the antenna elements for ALBA antenna elements and the arrayed configuration that forms the project breadboard have the objective of validating the design with the corresponding RF measurements as well as to address and quantify the functional-thermal performances of the design, and that is why the test campaign required in the ITT was mostly focused on thermal-functional aspects. This has been fully achieved with the test campaign.

The test campaign for the ALBA Breadboard includes :

- Dimensional testing, mass (T1).
- Bench test (T2,T4,T5), consisting on scattering parameter testing of the H + V ports of the individual antenna elements. The test includes both isolation and input matching terms at ambient and over the temperature from −10 to +40 degrees.
- Chamber test (T3): This test is performed in an anechoic chamber and consist on spherical near field pattern measurements of each of the elements included in the ALBA BB. The objective is the characterization of the antennas and the validation of their performances with respect to the pattern simulations. The patterns were conducted for all the antennas with a 90cmx90cm GP and the antenna placed close to its edge.
- Breadboard scattering parameters over temperature (T7) of the arrayed breadboard configuration of 11 antennas. Measurement were conducted in a thermal chamber at Airbus facilities to test scattering parameters between the ports of the BB, at different temperature scenarios ranging from −10 to +40 degrees.
- Array embedded radiation pattern (T8): This test is performed in an anechoic chamber and consist on spherical near field pattern measurements of each of the embedded pattern element in the ALBA BB array, with the effect of the coupling between neighbours. The objective is the characterization of the array and the validation of their performances with respect to the pattern simulations.

This final report includes a summary of the the main performances along the different tests, although for further clarifications or in-depth analysis, check RD5.

7.1 SINGLE ELEMENT RESULTS

7.1.1 T1 dimensional testing, mass

7.1.1.1 Dimensional Testing

This was performed with the results in line with general tolerances requested to the supplier.

7.1.1.2 Mass

The measurements of the mass of the 11 manufactured antennas gives a value of 155.67g and a std deviation of 0.58g, well in line with the expected values that was 154g [RD4]

7.1.2 T2: S parameter Test (individuals)

Scattering parameters for each individual antenna (represented by its serial number) were measured in ambient temperature, showing the following results. Uncertainty values for return loss is +/–0.35dB (1σ) in amplitude and +/–2º (1σ) in phase, and for transmission measurements it is +/-0.043dB (1σ) and +/-0.28º (1σ) for a reference S_{21} measurement of 0dB and +/–2dB (1σ) for a reference S_{21} measurement of –40dB. These uncertainty figures also apply to the measurements in T7 test.

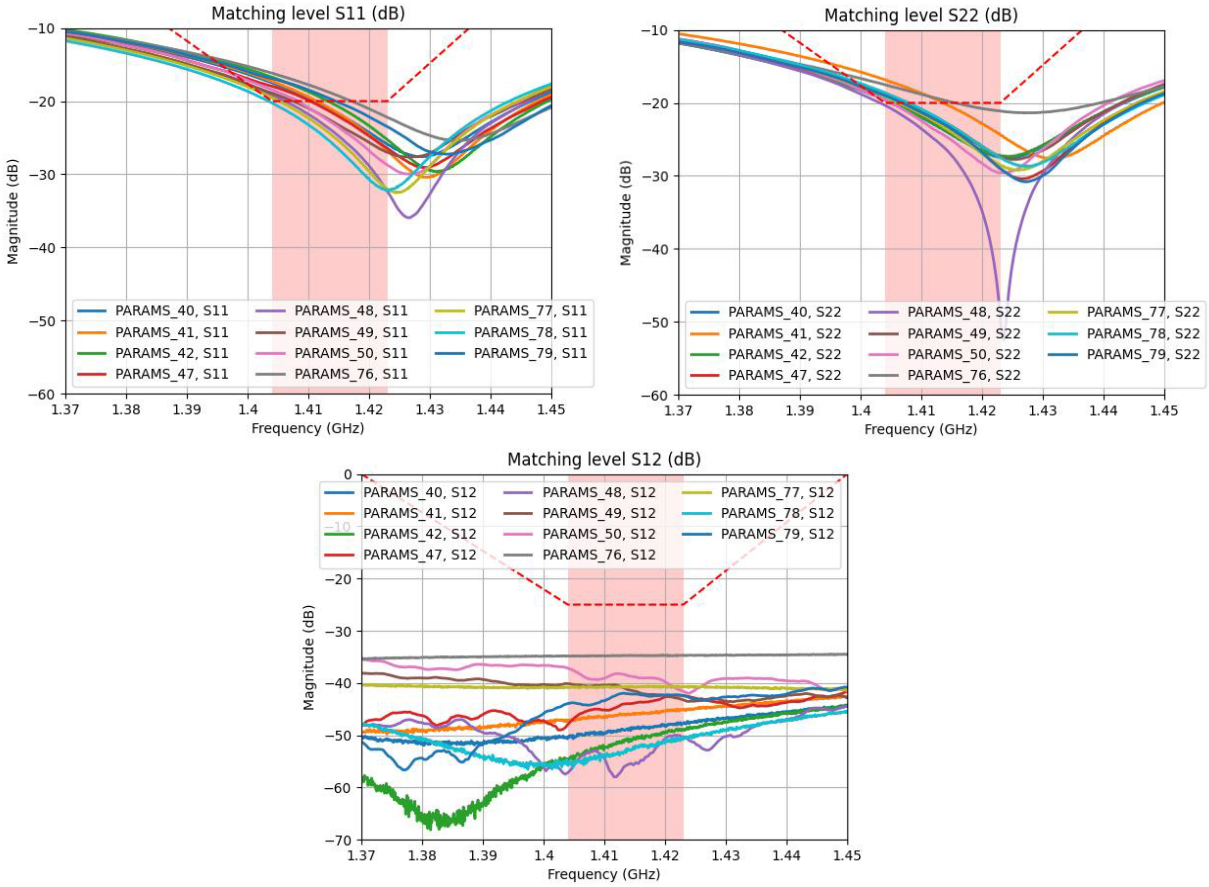

Figure 7-1: Measured S-parameters for each SN antenna for vertical polarization (S11) and horizontal polarization (S22).

7.1.2.1 Conclusions

Measurements indicate that there is some spread in the input match results that tend to shift to slightly higher frequency. The patch antenna repeatability has been manufactured with a general tolerance of +-0.3mm (produces an spread of about 10MHz wrt the centre value). The measurements indicate that disk patch size (extracted from CST simulations performance) should have been larger. A test unit with different patch size has been manufactured for validation (see Figure 7-2). In any case, this does not affect the results of the measurements and the conclusions of the test campaign. Port isolation is better than <–30dB in all cases and in the range of <–40dB for most of the elements, indicative of

adequate assembly of the parts of the antenna and the manufacturing of the balanced feeding PCB.

A study has been performed manufacturing different patch diameters, as increasing the patch diameter helps to center the performance with a input return losses below 20 dB in band (see Figure 7-2).

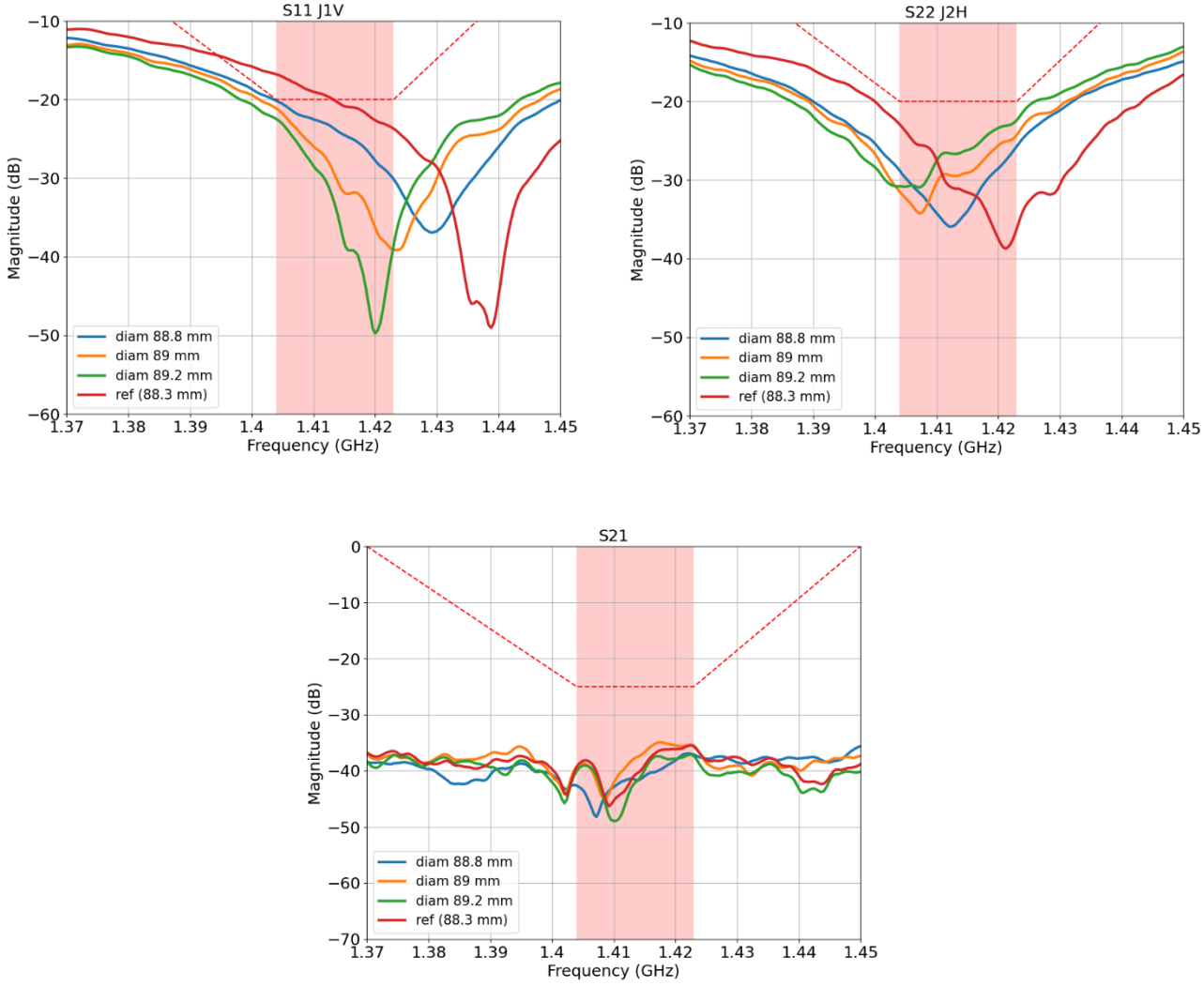

Figure 7-2: Measured S-parameters for different patch diameter in vertical polarization (J1) (S11) and horizontal polarization (J2) (S22), and port coupling (S21).

7.1.3 T3: Radiation Pattern Test (Individuals)

Radiation patterns of the 11 elements built to form the breadboard were measured in the UPM facilities with the antenna located at the edge of a square ground plane of 90cm × 90cm. The measurement reference frequency is 1413.5MHz. Data is also available at 1404MHz and 1423MHz and have been provided to UPC for system assessment simulations.

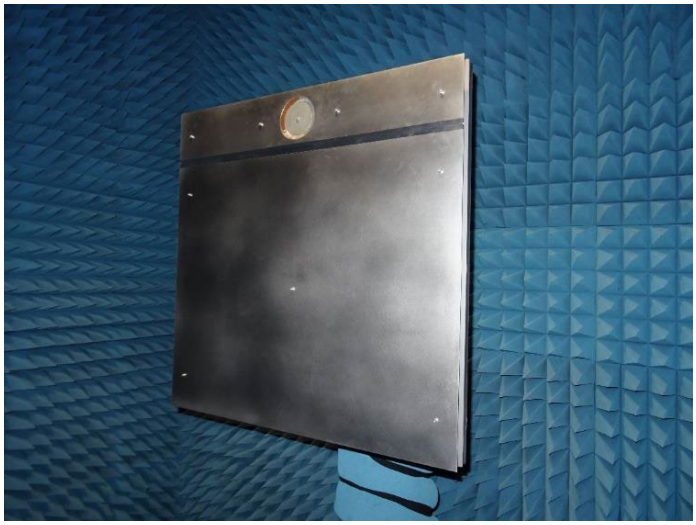

Figure 7-3: Antenna located at the edge of the ground plane

Figure 7-4 (left) shows the antenna ports locations. In all cases J1 corresponds to the vertical polarization and J2 to the horizontal polarization. The coordinate system for the radiation patterns measurements is shown in Figure 7-4 (right).

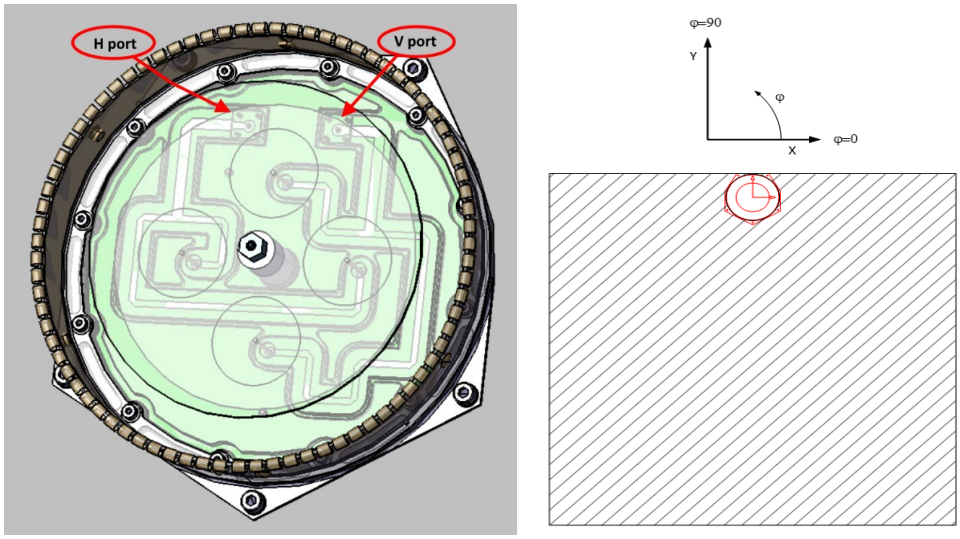

Figure 7-4 antenna element ports J1:V & J2:H

7.1.3.1 Radiation Pattern Measurements

Table 7-1 summarizes the main parameters for all the antennas and Figure 7-5 and Figure 7-6 show the copolar and crosspolar components versus simulation.

	Directivity at boresight (dB)		Copol(0,0)-Xpol (WC theta +-30) Ratio (dB)		BW3 phi=0 (deg)		BW3 phi=90 (deg)	
SN	polV	polH	polV	polH	polV	polH	polV	polH
40	8.11	7.69	19.23	21.59	73.21	75.53	75.23	76.52
41	8.02	7.68	20.71	21.35	74.53	75.62	73.37	76.26
42	8.07	7.72	22.30	20.91	74.18	75.32	74.25	75.67
47	8.00	7.63	19.73	20.20	74.95	80.66	74.38	75.65
48	8.02	7.62	21.27	20.10	74.77	81.19	75.56	76.34
49	7.95	7.64	19.17	19.98	75.29	78.86	74.58	75.99
50	8.08	7.66	21.64	20.57	75.27	79.44	72.57	76.2
76	8.09	7.64	23.73	20.54	75.36	80.36	79.57	76.41
77	8.08	7.63	20.39	20.35	75.29	80.47	72.98	76.43
78	8.06	7.65	21.55	20.89	74.66	80.41	80.41	76.17
79	8.09	7.62	22.28	20.48	75.67	81.12	78.41	75.85

Table 7-1: Antenna performance at the centre frequency (1413.5 MHz)

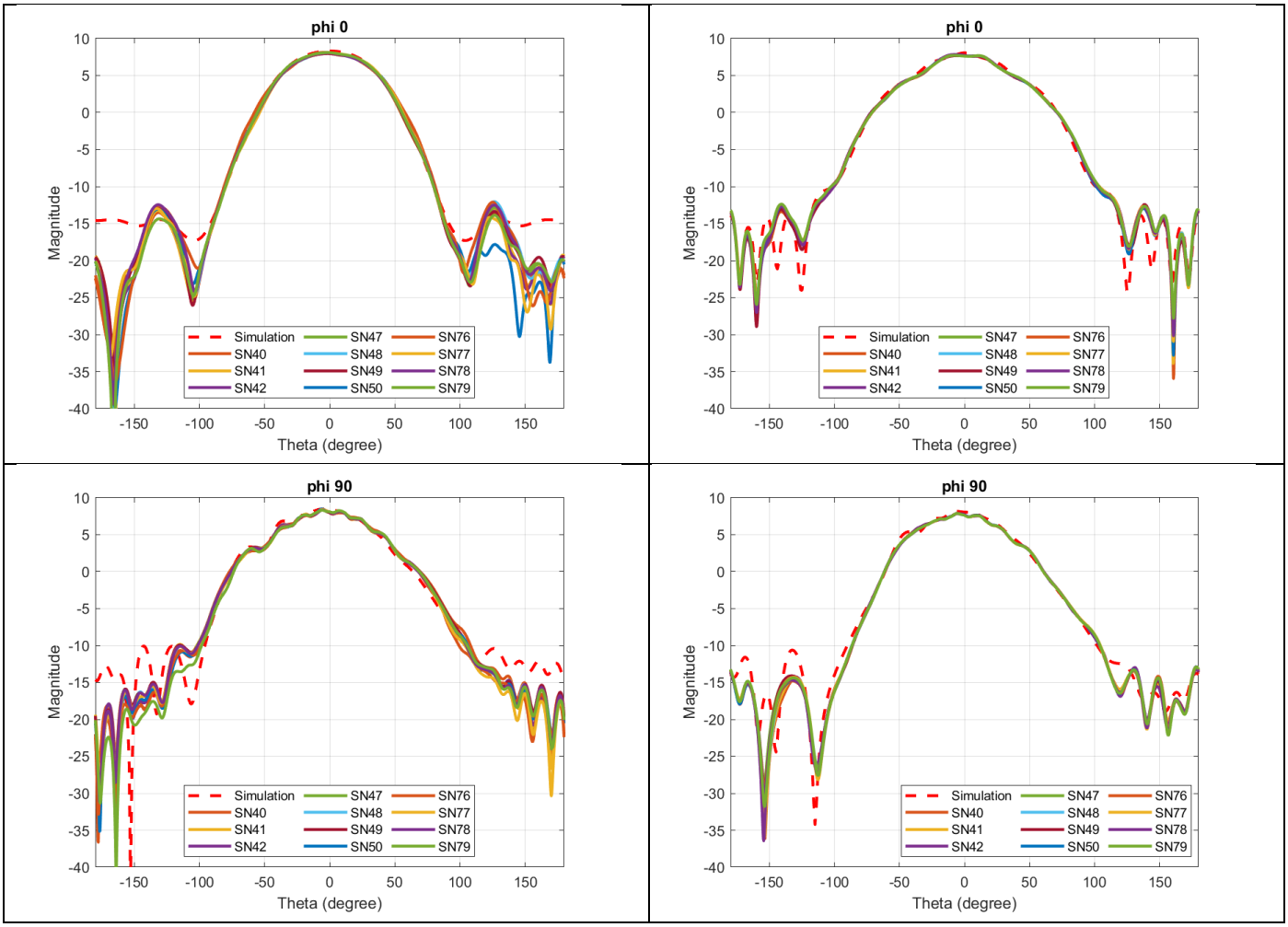

Figure 7-5 : Copolar component comparison for individual elements, left) vertical polarization (J1) and right) horizontal polarization (J2)

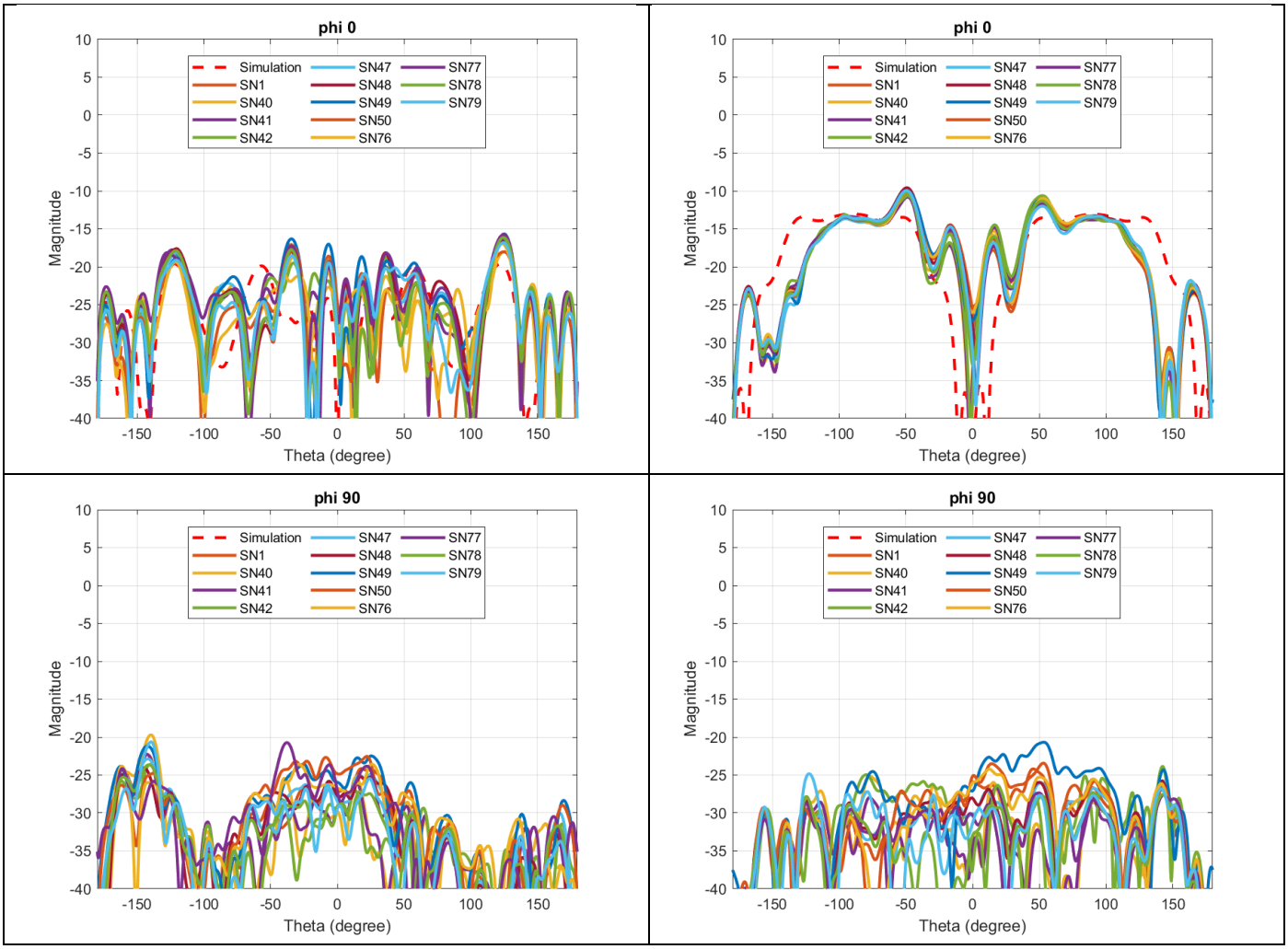

Figure 7-6 : Crosspolar component comparison for individual elements, left) vertical polarization (J1) and right) horizontal polarization (J2)

7.1.3.2 Deviation masks

The deviation masks, both for amplitude and phase are included for theta ranges, ±30°, along different phi-cuts. The figures show the result at the centre frequency (1413.5MHz)

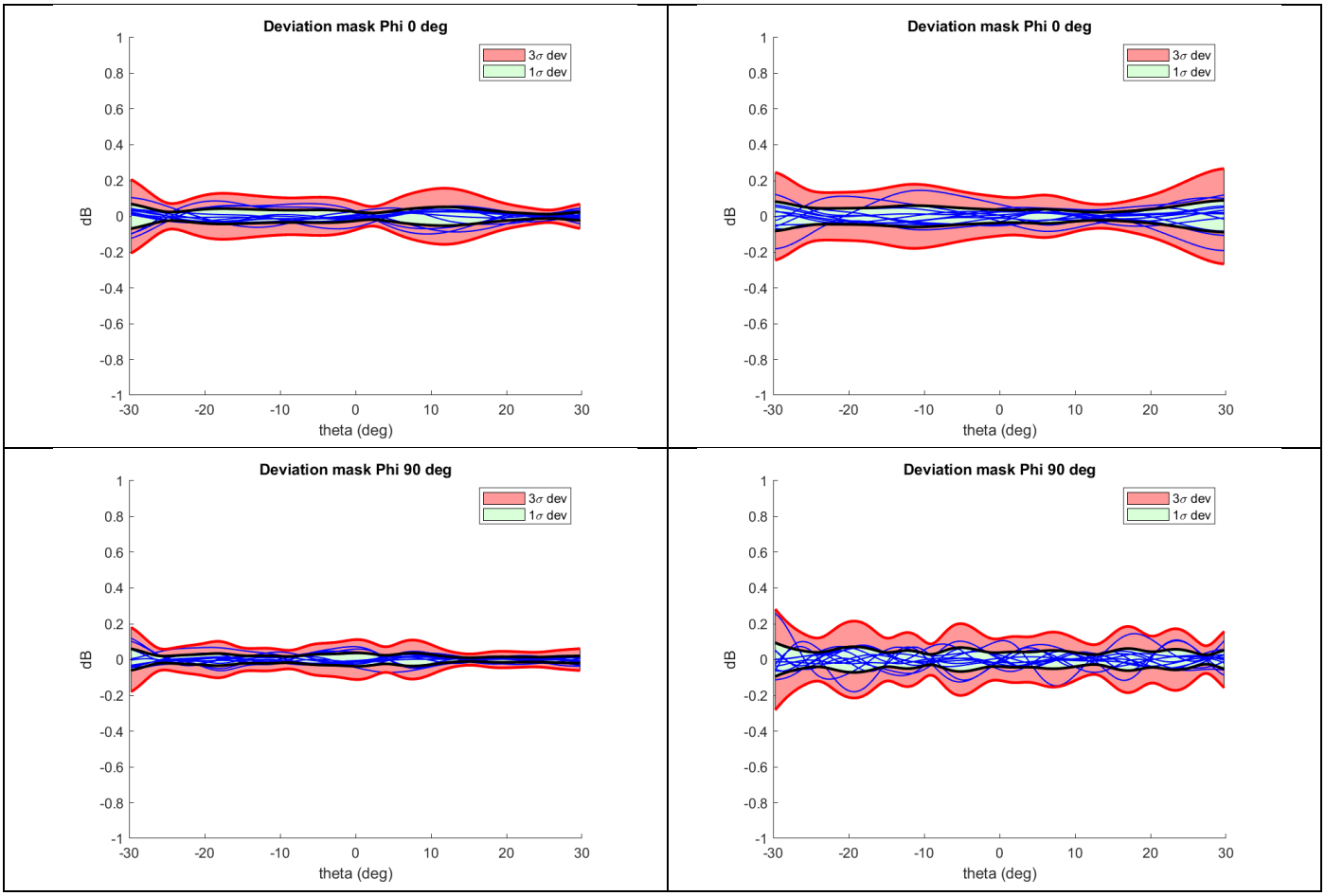

Figure 7-7 : Deviation mask in amplitude for (left) horizontal polarization and (right) vertical polarization

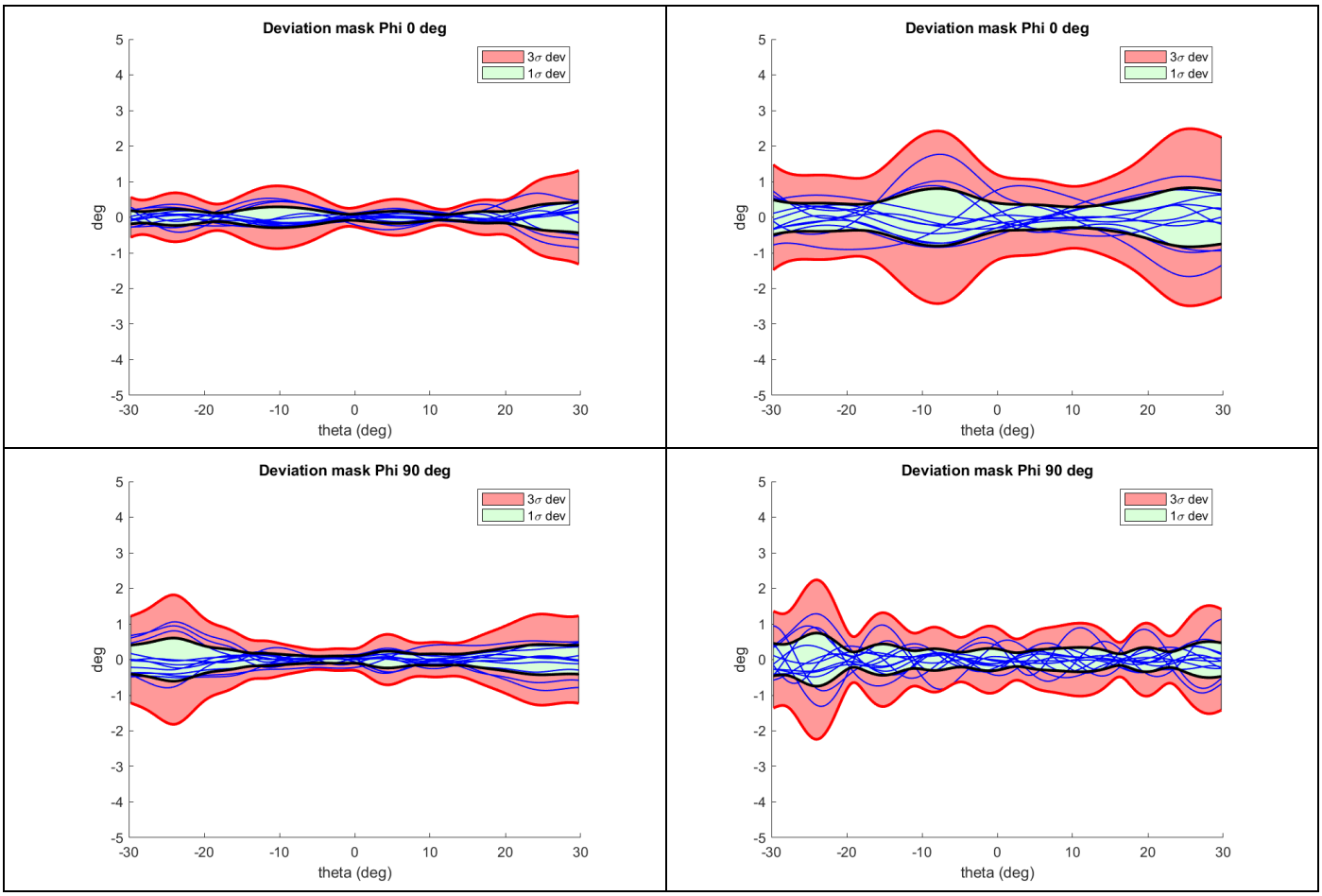

Figure 7-8 : Deviation mask in phase for (left) horizontal polarization and (right) vertical polarization

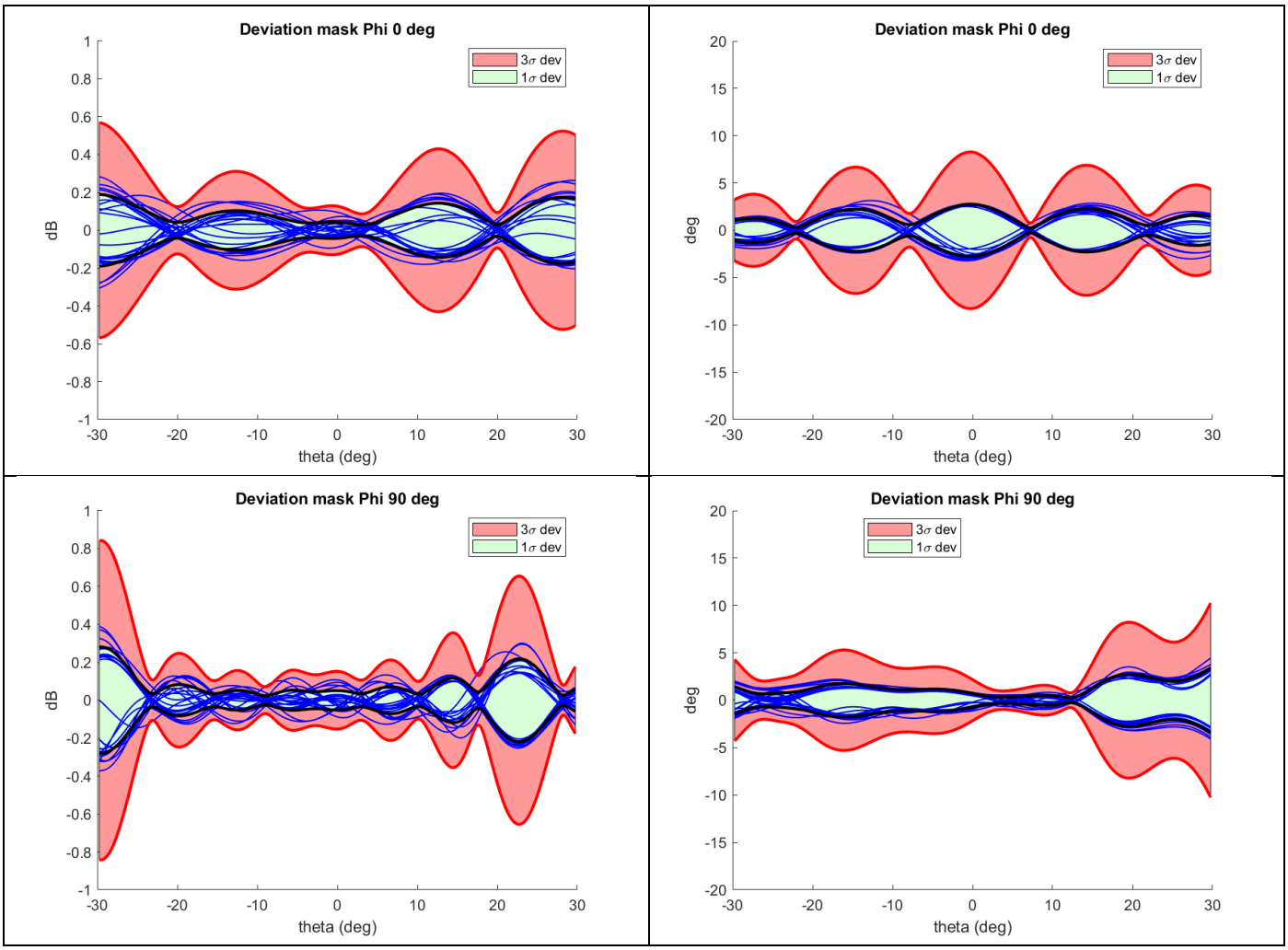

Figure 7-9 : Combined H & V (polarimetric) deviation mask for horizontal and vertical polarization theta range ±30° (left) for amplitude and (righ) phase.

7.1.3.3 Efficiency Measurements

In general, antenna gain measurement is usually performed at boresight, where the antenna AUT shows maximum gain, and the mounting of both the SGH and the AUT for the antenna testing implies that the antennas are centered in the spherical positioner of the test facility.

The uncertainty of the measurement is ±0.08dB(1σ)

Figure 7-10 shows a comparison for some isolated elements at different positions, centred in the ground plane (SGH and AUT aligned) and at the edge of the ground plane (SGH and AUT with a 5° misalignment). A correction factor was applied to correct the offset effect.

The centred configuration provides loss results fully in line with the expected values reported previously in [RD2,4,6,7], giving a value of less than 0.25dB. The probe pattern correction was applied to the edged results only, and the results show an excellent agreement between

the two set of data (offset and centred), indicating that the insertion loss of the antennas is well aligned with the conducted simulations.

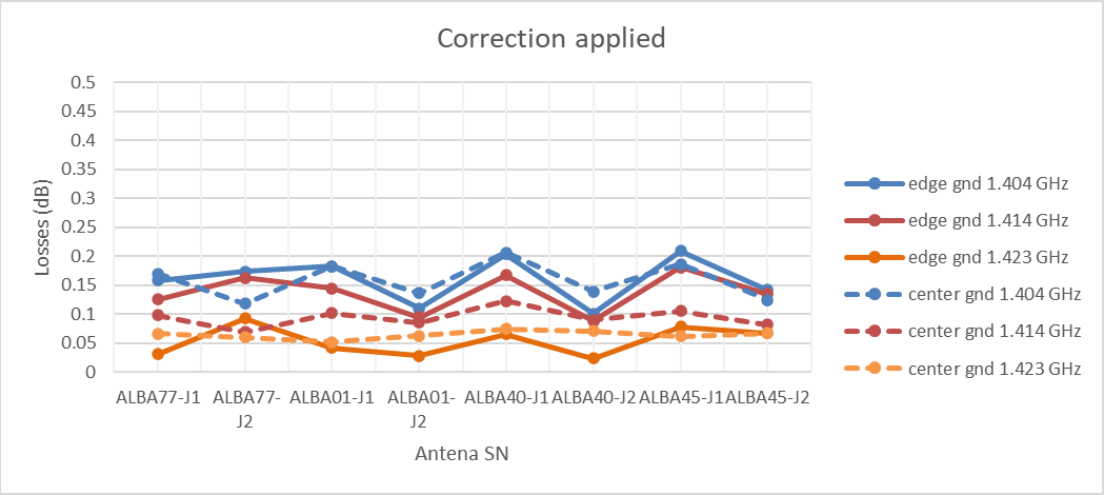

Figure 7-10: results of gain measurement investigation and antenna loss

7.1.3.4 Conclusions

Radiation patterns show very good repeatability for all the antennas. The test setup used, with the antennas located at the edge of a ground plane, has effects on the patterns that produce ripples in the copolar and crosspolar patterns. These ripples were properly simulated with CST.

The deviation masks applied to the individual antennas H and V gives a very good result of approximately +/-0.2dB (1σ) and +/-1deg (1σ) for Vpol and Hpol independently. When H and V are combined the spread increases up to +/-0.4dB (1σ) and +/-5deg (1σ), that reflects the fact that H and V pol ports are affected differently by the ground plane due to the different impact on each polarization of the ground plane position.

Finally, the loss measurements and discussion took more time than initially planned due to the boresight offset effect that was not initially considered and implied the manufacturing of a centred setup that allow to solve the discrepancies. In conclusion the gain/directivity technique to determine the loss of the antenna has shown to be valid with the associated uncertainty. The value obtained is better that 0.25dB including mismatch [RD5]

In conclusion, the alignment between the CST simulations and the measurements is excellent both in copolar and crosspolar patterns.

7.1.4 T4 S-Parameter Vs Temperature (2 individuals)

Two of the manufactured antennas (SN47 and SN48) were measured in temperature with a set of thermocouples attached to the cavity. For more information please check RD5.

Figure 7-11 antenna element inside the thermal chamber covered with absorbers

The temperature profile for the test followed a 10 degree step as: T20°C→ -10°C → 0°C → 10°C → 20°C → 30°C → 40°C → 20°C.

The calibration of the VNA was performed at the input plane of the antenna with SMA. Test setup results therefore include SMA-SMP transitions (negligible effect). Also, the cables used in the measurement were characterized in the thermal range and their effect taken into account.

The following figure shows the S-parameter variation for the test resulting in a low sensitivity versus temperature (only SN47 is shown although applies to SN48 as well).

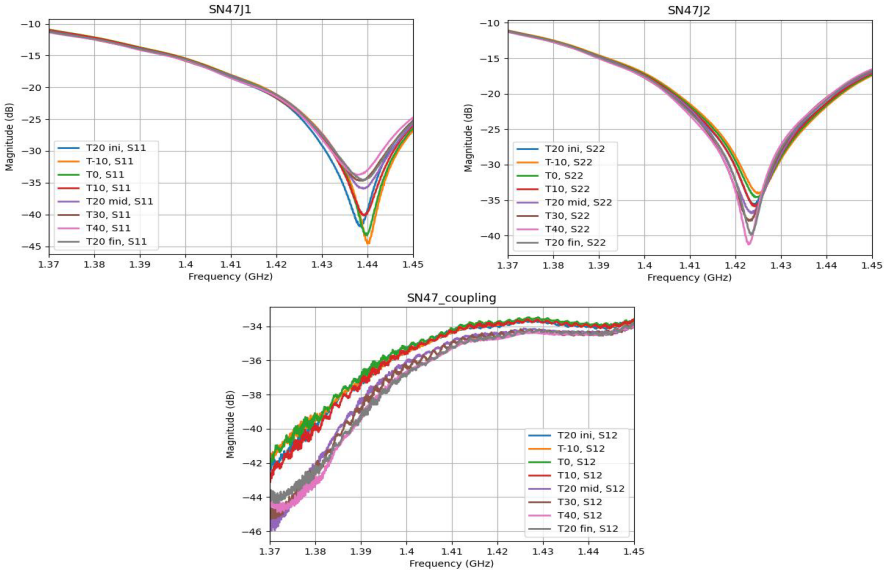

Figure 7-12: reflection and isolation between ports vs temperature (SN47)

7.1.4.1 Conclusions

The tests performed show the low sensitivity vs temperature of input match and port to port isolation of the ALBA antennas.

7.1.5 T5: Insertion Amplitude/Phase Vs Temperature

SN47 and SN48 were also used to measure the S-parameter results in a face to face configuration to determine the transmission term versus temperature. Tests were also conducted at a thermal chamber in Airbus facilities.

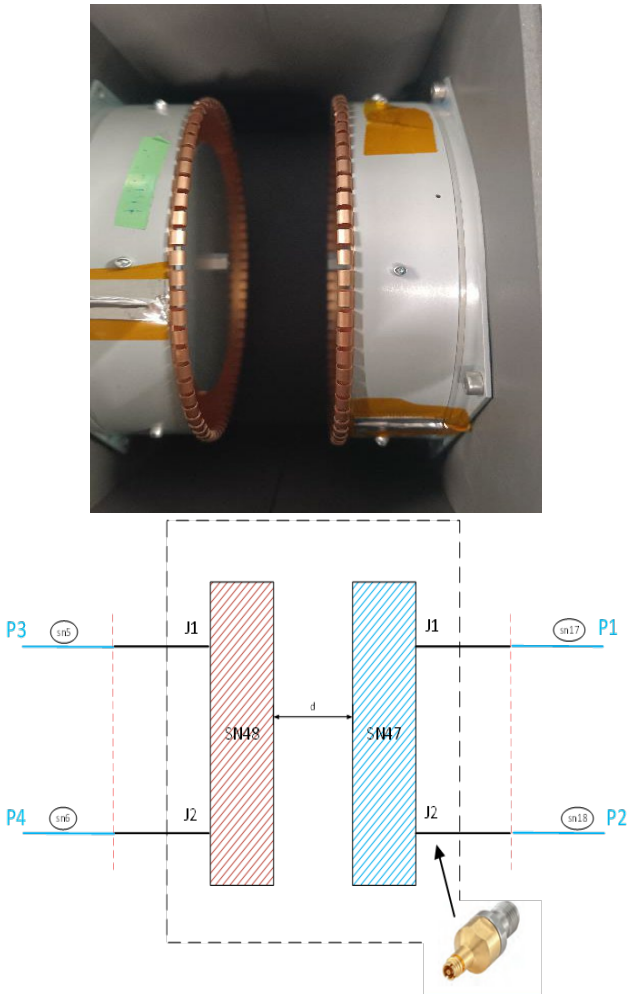

Figure 7-13 photographs of the face-to-face setup assembly. The metallic housing is internally covered with eccosorb SF absorber

From Figure 7-14, the transmission variation with respect the initial reference measurements (T=20ºC) have been represented. From this figure it can be derived that the variation of the measurement within the operating band is less than the required +/-0.05dB, which implies that the variation of each antenna is in the range of +/-0.025dB. In the case of the phase the variation in the thermal range is less than +1º (only shifts in the positive sense) and therefore the single antenna variation is less than +0.5º, compatible with the requirement. Thus, it is noticed the limited effect of the thermal excursion.

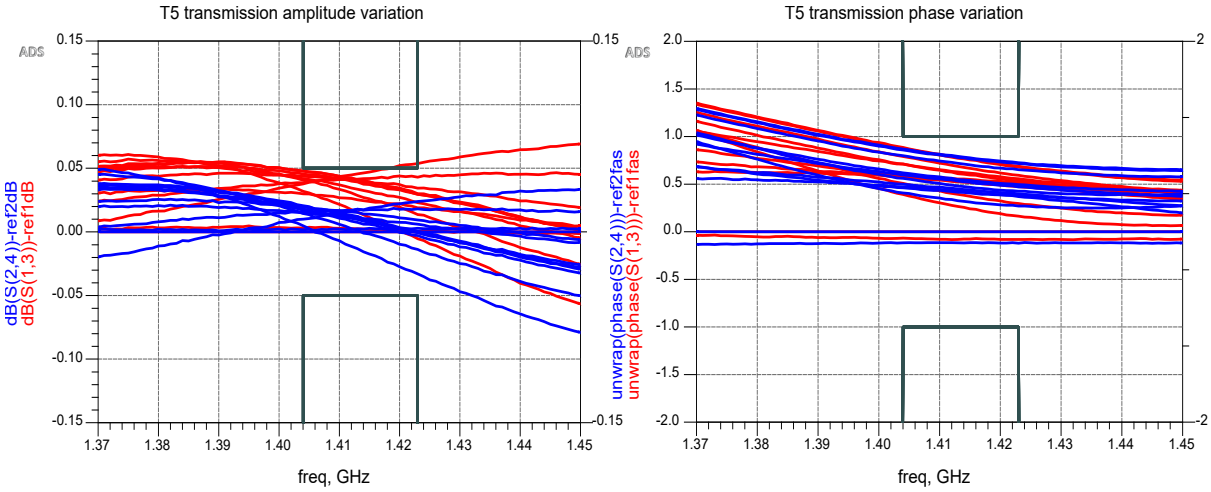

Figure 7-14: Variation of transmission parameters vs temperature and frequency in face-to-face test

7.1.5.1 Conclusions

T5 summarizes that Face-to-Face data showed a small variability of the ALBA antenna design in temperature. This test completes the tests performed in T4 in which the sensitivity of input match and port to port isolation of individual antennas has been shown to be very small. In conclusion, the requirement on temperature stability of the antenna design is considered fulfilled.

7.1.6 Single Element Conclusion

The antenna element for the ALBA project has been analysed in detail. All major and relevant aspects of the antenna and its assembly on the planned TriHex Instrument have been studied. The impact of the expected location of the antenna close to the edge of the Instrument have been analysed and measured, both for an individual element and for the elements of the complete array. Coupling effects within the elements have been analysed and their effect on the radiation pattern has been shown.

Test results have shown the small variability of the ALBA antenna design in temperature. The tests performed in T4 and T5 in which the sensitivity of input match and port to port isolation and the internal transmission has been shown to be very small. In conclusion, the requirement on temperature stability of the antenna design is considered fulfilled.

7.2 ALBA ARRAY BREADBOARD

The ALBA Breadboard consists of a set of 11 antennas of ALBA array designed for the TriHex Instrument (see Figure 7-15), arranged in the perimeter of the structure with the distribution of the polarization ports as shown in the figure.

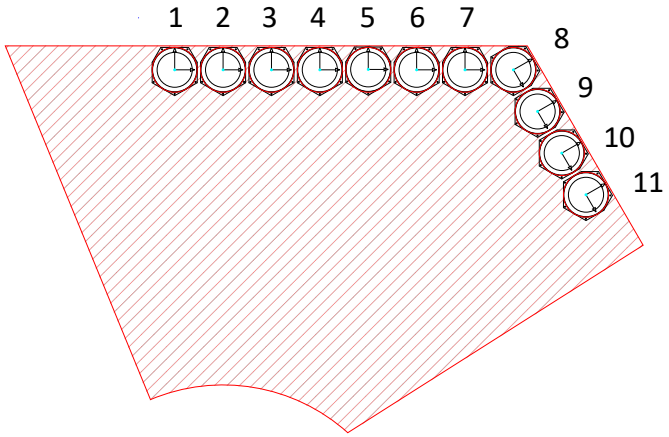

Figure 7-15 definition of TriHex-SMOS radiating subsystem with radiating elements used in the BB of the antenna Instrument

The setup allows the characterization of the coupling terms between the elements in the arm and the coupling terms between the elements of two different arms, and it also allows to measure the radiation patterns of the elements embedded in the array and test the effects of the edges as well as the effect of the central cylindrical cut-out on the radiation pattern. A large ground plane is required for validation of the effect of the boundary conditions on the antenna pattern.

7.2.1 T7: Scattering parameters results over temperature

This sections includes the S-parameter measurement over temperature for the breadboard (T7) and the radiation pattern measurement (T8).

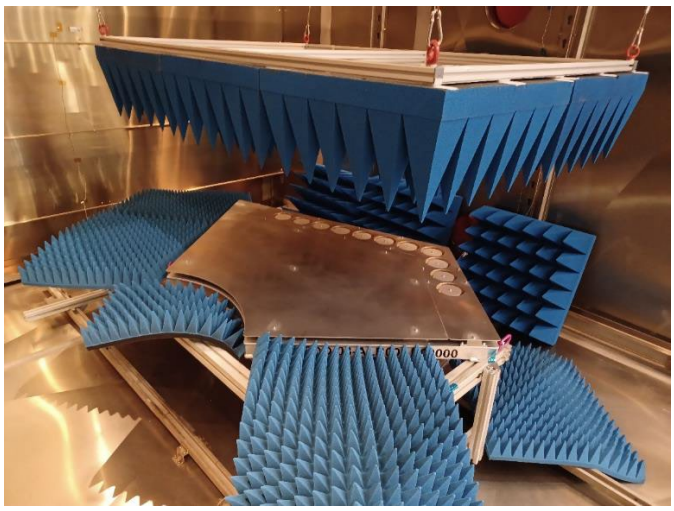

Figure 7-16 thermal chamber photograph for T7 test

Scattering parameters have been tested for all the array elements, in H-H, V-V as well as in V-H and H-V configurations, using a 1:32 switching matrix. Reference cables were also included and measured in the setup to deembed the effect of the cables in the measurements.

VNA calibration planes were located at the switch matrix ports connected to the DUT. The deembedding process was successfully performed in the transmission coefficients (amplitude and phase).

For the coupling terms and after the deembeding process of test cables, the results were in agreement with the simulations as shown in Table 7-2 to Table 7-5 (T=20ºC mid).

As summary, data in the complete thermal range are included Figure 7-17 with a comparison of the different coupling terms with temperature, for the antenna SN04 and SN08, compared to its neighbours elements.

7.2.1.1 Coupling terms in temperature range (-10ºC to +40ºC)

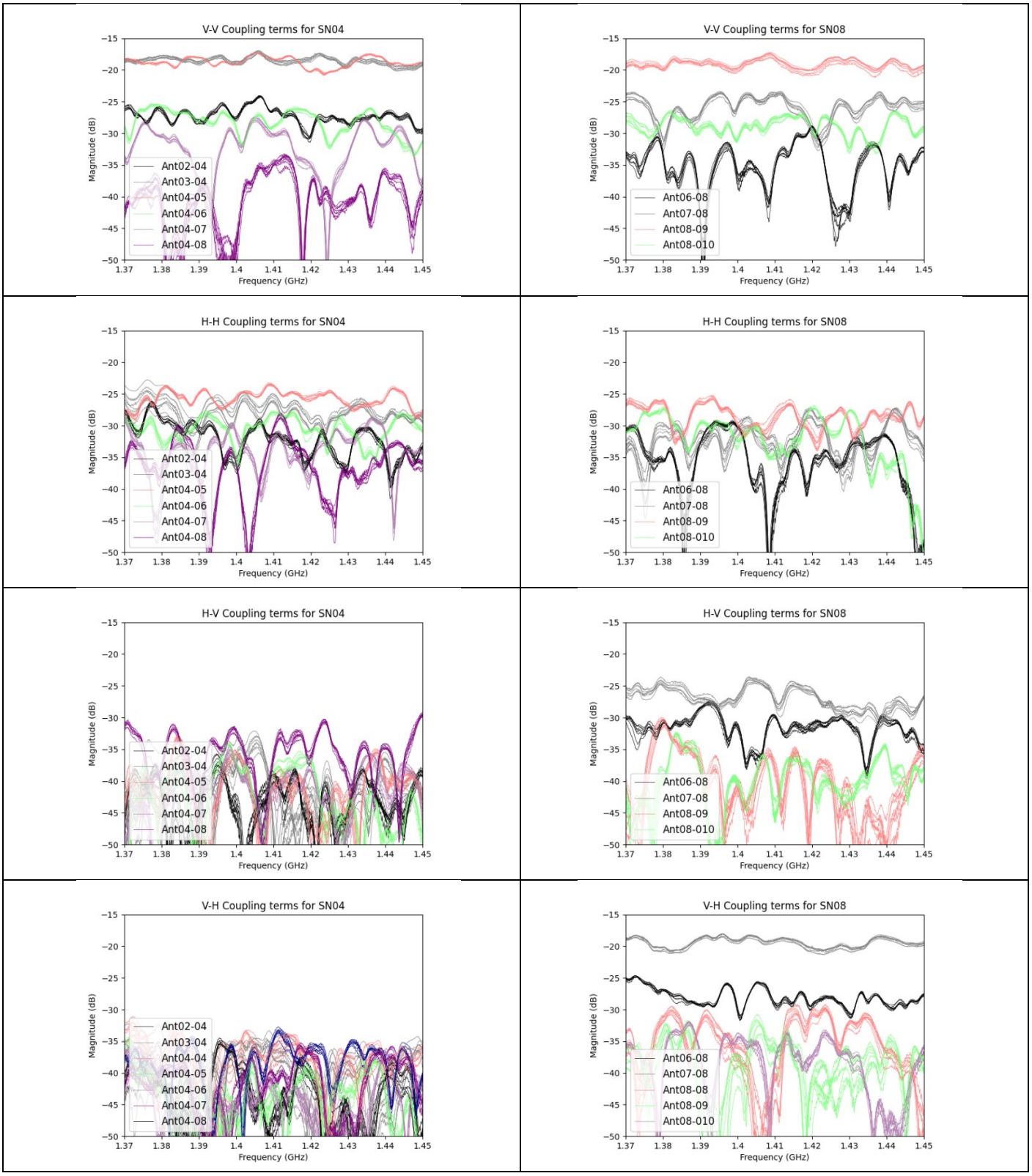

Figure 7-17: Measured coupling terms for SN04 and SN08 (T=–10ºC to +40ºC)

7.2.1.2 V-V coupling terms

As expected from the simulations performed with the 3D CST EM model, the largest coupling term occurs between close neighbours and it is in the –18dB range. This is replicated in all elements aligned in the same J1 (V) polarization. For elements with tilted polarizations (#7-#8), the different orientation produces additional reduction (to –25dB as simulated with CST), and comes back to –18dB between tilted antennas (#8-#9).

Measurement vs Simulated values (dB)	SN01	SN02	SN03	SN04	SN05	SN06	SN07	SN08	SN09	SN10	SN11
SN01		17/18	25/24	30/30	30/36	30/42	35/48	35/57	35/50	35/51	35/50
SN02			17/18	25/23	27/30	35/36	35/41	35/53	35/48	35/47	35/48
SN03				17/18	25/23	25/29	30/36	35/50	40/44	35/44	40/45
SN04					17/18	25/23	27/30	35/44	35/39	35/40	35/42
SN05						17/18	25/24	35/37	35/34	35/37	35/39
SN06							17/18	30/30	30/30	30/33	35/37
SN07								25/24	25/26	30/30	35/35
SN08									17/18	25/24	30/31
SN09										17/18	25/24
SN10											17/18
SN11											

Table 7-2: Comparison of coupling terms V-V for measurement/simulation

7.2.1.3 H-H coupling terms

Also, as expected from the simulations performed, the largest coupling term occurs between close neighbours and it is in the –25dB range. This is replicated in all elements aligned in the same J2 port, (H) polarization. For elements with tilted polarizations (#7-#8) the different orientation produces additional reduction (to –30dB), and comes back to –25dB between tilted antennas (#8-#9).

Measurement vs Simulated values (dB)	SN01	SN02	SN03	SN04	SN05	SN06	SN07	SN08	SN09	SN10	SN11
SN01		25/28	27/29	30/30	30/33	30/36	30/40	35/49	35/47	35/48	35/52
SN02			25/28	27/29	30/30	30/33	35/37	30/45	30/44	30/45	35/48
SN03				25/28	30/29	30/30	30/34	35/41	35/41	35/41	35/44
SN04					25/27	27/29	30/30	30/38	35/38	35/38	35/40
SN05						25/27	30/28	30/34	30/33	30/34	30/37
SN06							25/27	30/34	30/30	35/30	30/34
SN07								30/33	30/30	35/29	35/33
SN08									25/28	27/28	27/30
SN09										23/28	25/29
SN10											23/27
SN11											

Table 7-3: Comparison of coupling terms H-H for measurement/simulation

7.2.1.4 V-H coupling terms

VH couplings are in general small compared to the VV and HH, and the effect on the pattern is very small. Orthogonal coupling terms are in the range of –40dB. The largest coupling term occurs between elements of contiguous arms (e.g. #7 and #8).

Measurement vs Simulated values (dB)	SN01	SN02	SN03	SN04	SN05	SN06	SN07	SN08	SN09	SN10	SN11
SN01	33/53	40/46	35/48	35/51	35/56	35/64	35/77	35/60	30/56	30/51	35/50
SN02		35/60	35/48	35/48	35/50	35/55	35/59	35/49	35/52	35/48	35/48
SN03			35/66	35/49	40/48	35/49	35/50	35/43	40/50	35/45	40/45
SN04				30/67	40/48	35/46	35/47	35/36	35/46	35/42	35/42
SN05					32/67	35/46	40/44	30/31	30/42	30/40	30/40
SN06						32/54	35/44	25/25	30/35	30/36	30/37
SN07							30/48	17/19	25/30	25/32	30/33
SN08								30/42	30/48	35/49	35/49
SN09									35/37	35/47	35/49
SN10										32/37	35/53
SN11											

Table 7-4: Comparison of coupling terms V-H for measurement/simulation

7.2.1.5 H-V coupling terms

HV couplings are show the same behaviour than VH terms, and they are, in general, small compared to VV and HH, therefore their effect is expected to be very small. Orthogonal coupling terms are in the range of –40dB as in VH. The largest coupling term occurs between elements of contiguous arms (e.g. #7 and #8) .

Measurement vs Simulated values (dB)	SN01	SN02	SN03	SN04	SN05	SN06	SN07	SN08	SN09	SN10	SN11
SN01		35/55	35/49	35/50	35/53	35/54	35/58	35/45	35/49	35/48	35/47
SN02			35/51	35/49	35/49	35/51	30/55	30/42	30/45	30/45	35/45
SN03				30/50	35/48	40/50	35/53	30/39	40/41	35/42	35/42
SN04					35/27	35/29	35/30	30/38	30/37	35/37	35/40
SN05						35/56	35/54	30/31	30/34	30/37	30/40
SN06							35/68	30/30	30/32	35/36	35/40
SN07								25/29	25/31	30/35	30/42
SN08									35/42	35/43	35/45
SN09										35/41	35/44
SN10											35/43
SN11											

Table 7-5: Comparison of coupling terms H-V for measurement/simulation

7.2.1.6 Conclusions

As it has been shown in the results, simulations done in CST and measurement are in excellent agreement as indicated in the table results. Furthermore, the different coupling terms are insensitive to the temperature variation from −10ºC to +40ºC, which implies that the variation with the temperature of the antenna is negligible as expected from previous analysis in T4 and T5 (see sections 7.1.4 and 7.1.5). In summary, this translates in the conclusion that the antenna element construction and design is very stable with the temperature and coupling terms between them are not affected by the thermal excursion.

7.2.2 T8 array embedded element patterns

The radiation patterns that are shown in this section were measured at DTU anechoic chamber facilities (see Figure 7-18).

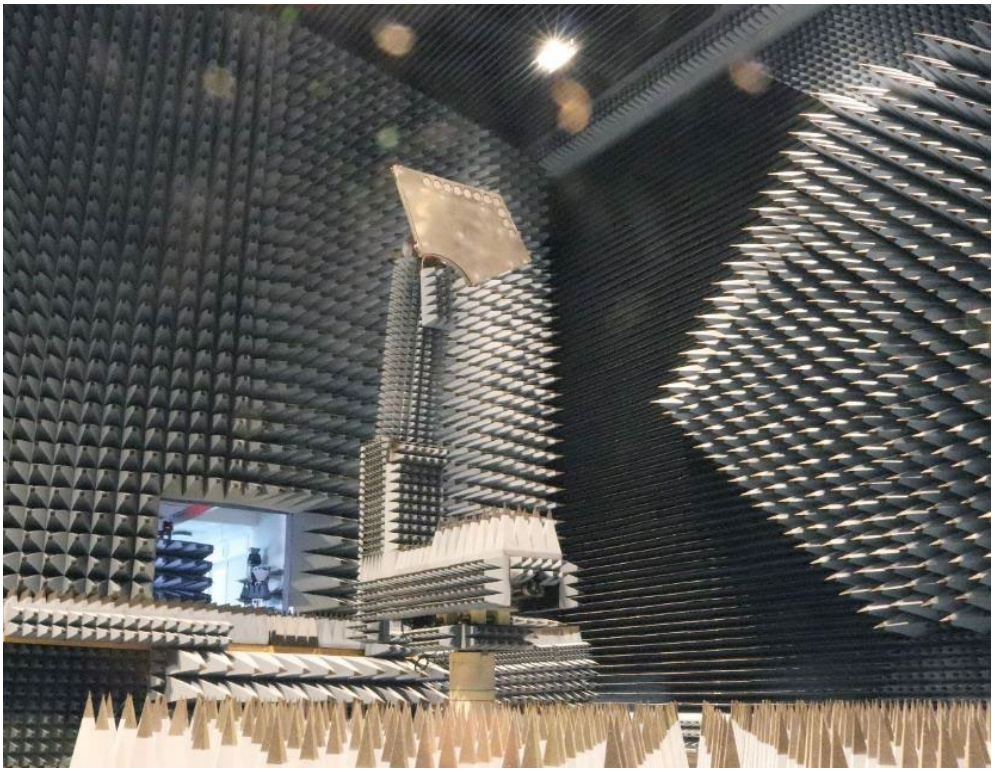

Figure 7-18 photograph of ALBA complete breadboard at DTU test chamber.

Radiation patterns were translated and rotated from the measurement coordinate system, located at the I/F plane with the tower mast, to each of the local coordinate systems of the radiating elements (as depicted in Figure 7-19) which are located at the centres of each patch antenna. This allows calculation of similarity masks between them.

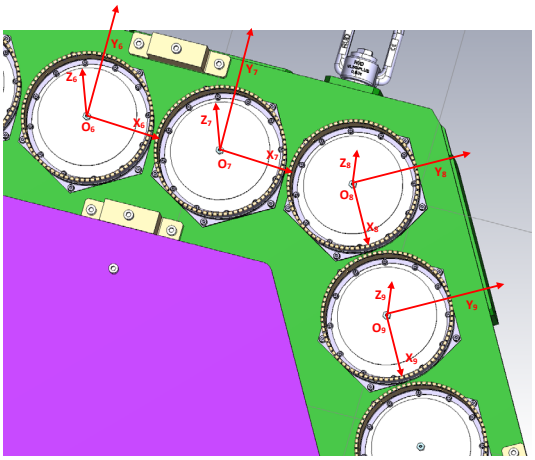

Figure 7-19 elements orientations and local coordinate systems

7.2.2.1 Radiation Pattern Measurements

This section includes the radiation pattern results measured at DTU. As other patterns that are included in this report, results are shown at the centre frequency (1413.5MHz) although data are also available at the band edges (1404MHz, 1423MHz). It is noticeable that the embedded patterns include the effect of mutual coupling terms between antennas which have been shown in previous section 7.2.1.

Table 7-6 summarizes the main parameters for all the antennas in the breadboard configuration, and Figure 7-20 and Figure 7-21 show the copolar and crosspolar components.

	Directivity at Boresight (dB)		Co(0,0)-Xpol (WC ±30deg) Ratio (dB)		BW3 phi=0 (deg)		BW3 phi=90 (deg)	
SN	polV	polH	polV	polH	polV	polH	polV	polH
1	7.96	7.69	24	19	89.10	88.59	67.99	74.51
2	6.80	7.19	20.7	20.9	103.86	97.73	73.50	73.86
3	7.13	6.86	21.5	19.9	104.55	94.84	67.38	75.06
4	7.02	7.58	22.3	20.1	105.97	87.93	68.58	72.02
5	7.19	6.61	24.6	20.3	107.92	93.46	69.22	74.48
6	6.63	7.37	24.4	19.2	104.80	95.44	77.62	74.44
7	7.25	6.97	23	17	102.65	95.64	65.57	73.75
8	6.89	7.24	19.1	15.4	96.08	82.00	87.23	87.12
9	7.12	6.27	25.7	16	102.09	84.95	71.44	76.40
10	6.92	7.49	23.1	19.9	101.65	91.28	72.53	69.19
11	7.62	7.32	24.1	19.7	89.34	88.43	71.00	77.61

Table 7-6: Breadboard array elements performances at centre frequency (1413.5MHz)

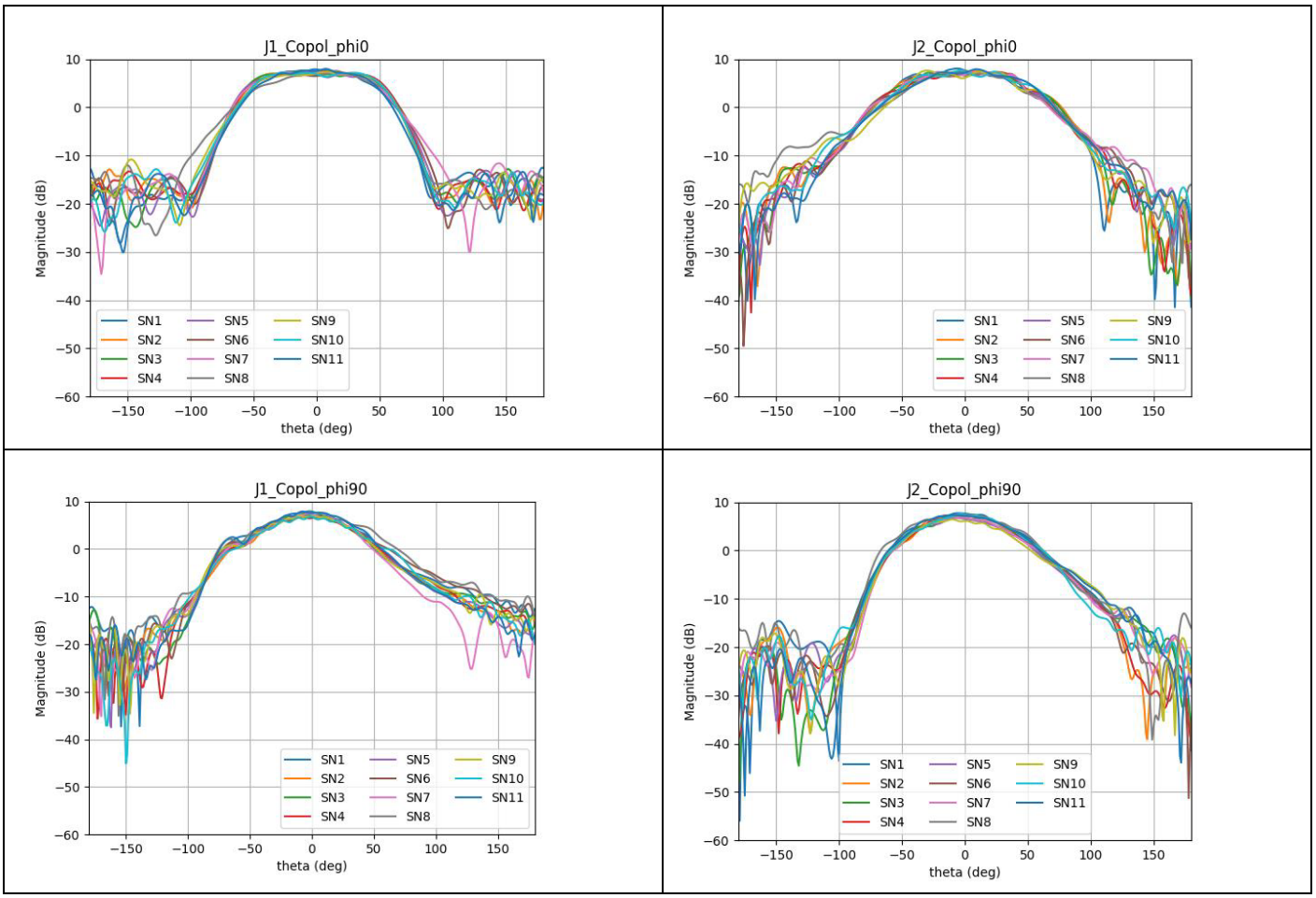

Figure 7-20 : Copolar radiation pattern for the complete set of breadboard antennas

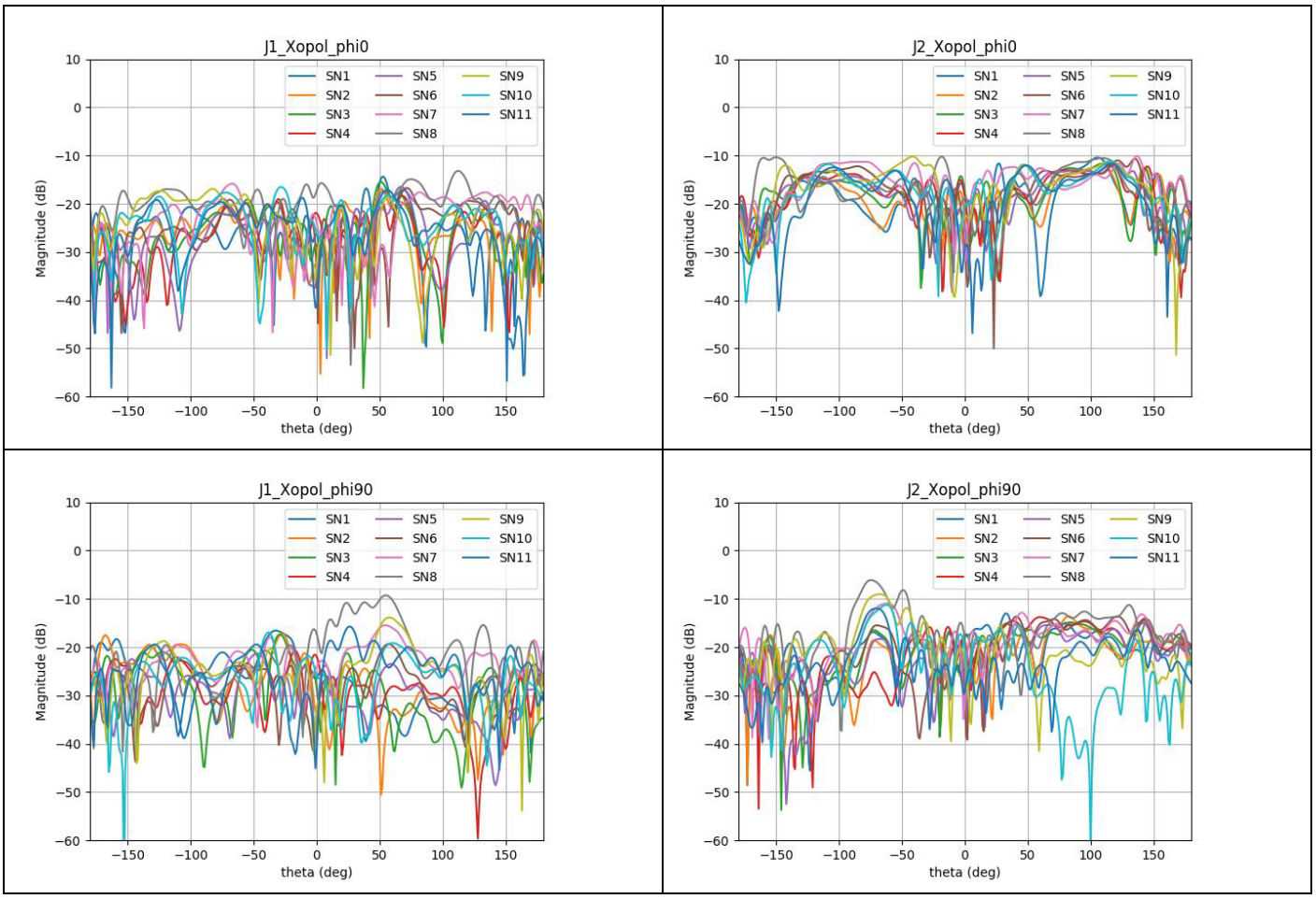

Figure 7-21 : Crosspolar radiation pattern for the complete set of breadboard antennas

7.2.2.2 Deviation Masks

The deviation masks, both for amplitude and phase have been computed and are included for theta ranges ±30°, along different phi-cuts. The figures show the result at the centre frequency (1413.5MHz)

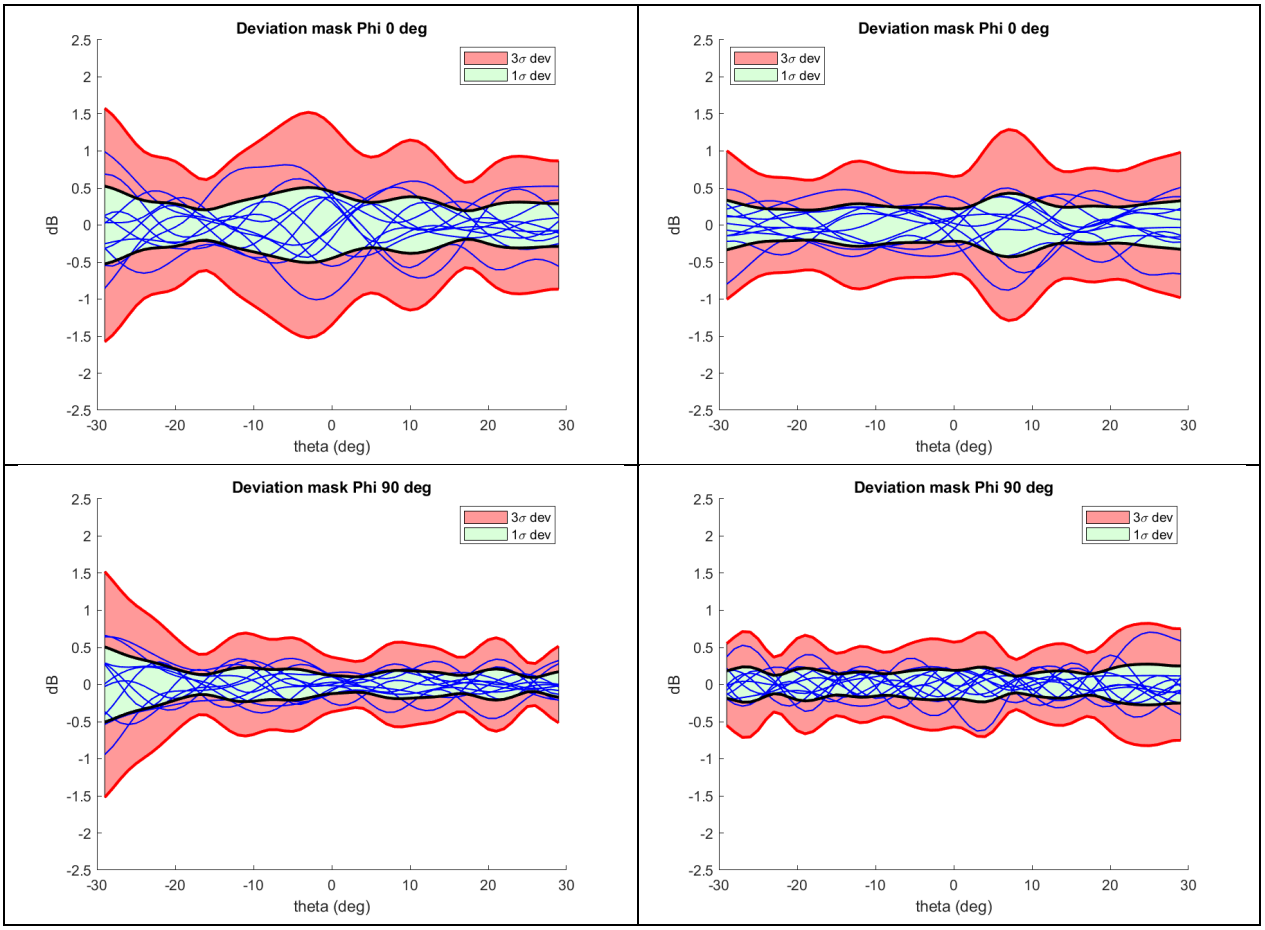

Figure 7-22 : Deviation mask in amplitude for (left) horizontal polarization and (right) vertical polarization

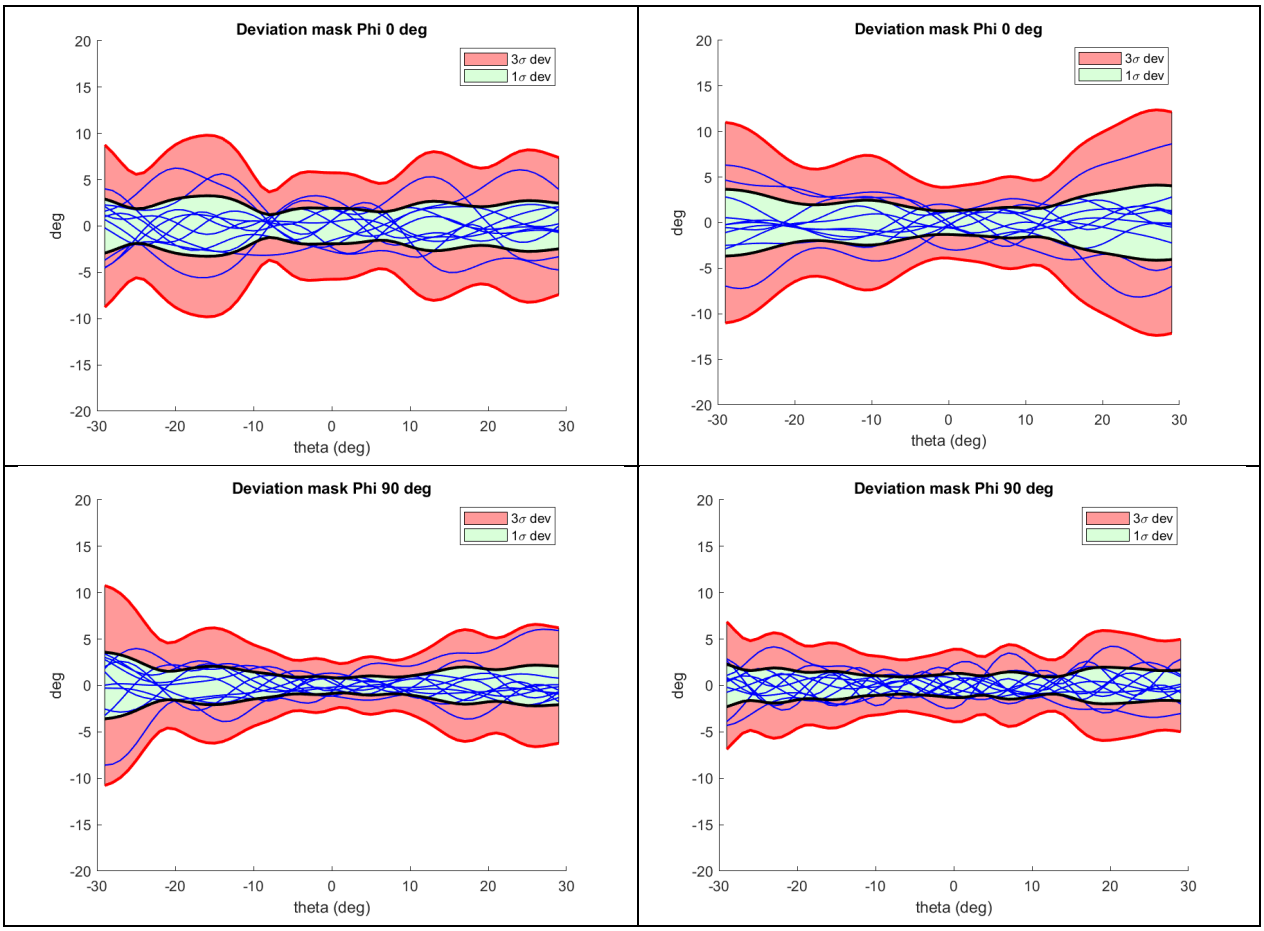

Figure 7-23 : Deviation mask in phase for (left) horizontal polarization and (right) vertical polarization

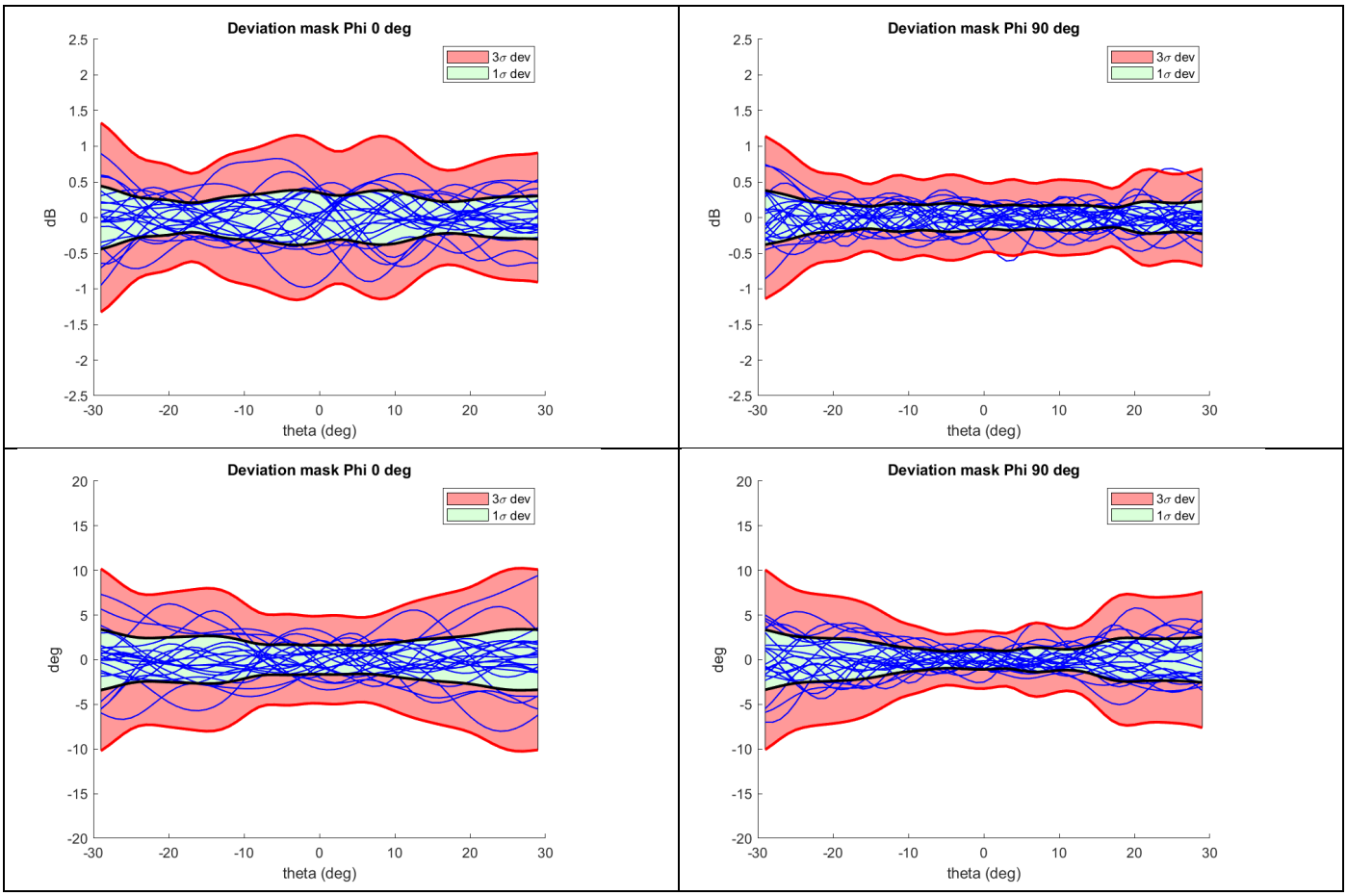

Figure 7-24 : Combined H & V (polarimetric) deviation mask for horizontal and vertical polarization theta range ±30 (left) in amplitude and (right) in phase

The antennas show an excellent degree of similarity for H and V, in the range of 0.5dB(1σ) in amplitude and 3º(1σ) in phase, even with the effects due to the asymmetry of the array configuration and the different positions of the antennas in the setup.

In polarimetric mode (which is designated as 'combined' H&V in previous figures), the deviation mask shows a larger dispersion which is a direct result of the sensitivity of the pattern components to the position close to the edge of the ground plane.

7.2.2.3 Efficiency Measurements

The breadboard antenna efficiency values were measured at DTU. In this case, losses for J2 (horizontal polarization port) are in agreement with previous antenna efficiency measured for the isolated elements (see section 7.1.3 and Figure 7-10), and losses for J1 show larger dispersion.

In the breadboard configuration (see Figure 7-25), the J1 (vertical polarization port) exhibits higher losses values than J2 (by ~0.15dB). This fact was analyzed in RD5 and has been also noticed in section 6.2 of this document, and is related to the higher coupling terms for V-polarization than in H-polarization (−18 dB for V-pol between close terms and −25 dB for H-

pol, which gives approximately $dB(\sqrt{1-2\times(10^{-18/20})^2}) = -0.14dB$ added loss assuming only the two closer neighbours have an influence, which is consistent with the efficiency of 0.4dB measured in J1. For the J2 (Hpol) the effect of coupling is less than -0.028dB, with respect the isolated case, which is not noticeable in the gain measurement or in section 6.2.

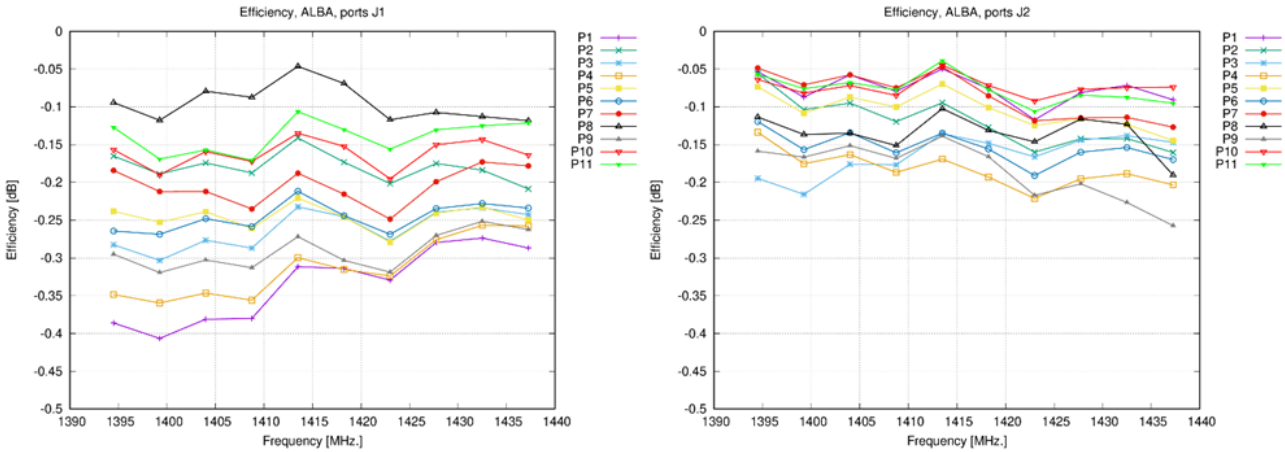

Figure 7-25: Breadboard efficiency values measured at DTU for: left) vertical polarization and right) for horizontal polarization

7.2.2.4 Array Breadboard Conclusions

Radiation patterns have been measured for each of the antenna elements that form the 11-element breadboard array. Three frequencies have been measured for each antenna port in copolar and crosspolar (H & V). The embedded conditions affect the peak directivity as well as the efficiency with respect the isolated condition measurements shown in section 7.1.3.

In the array case, the close spacing between antennas (122mm=0.577λ) causes the V-V coupling to be large and this gives place to a reduction of the peak directivity (and gain) of the V polarization of the antennas, while the directivity of the H pol is less affected.

As it is shown in the Figure 7-26 the effect is noticeable in the elements that are situated in 'more embedded' positions, while the elements that are at the edges of the array are affected less pronouncedly.

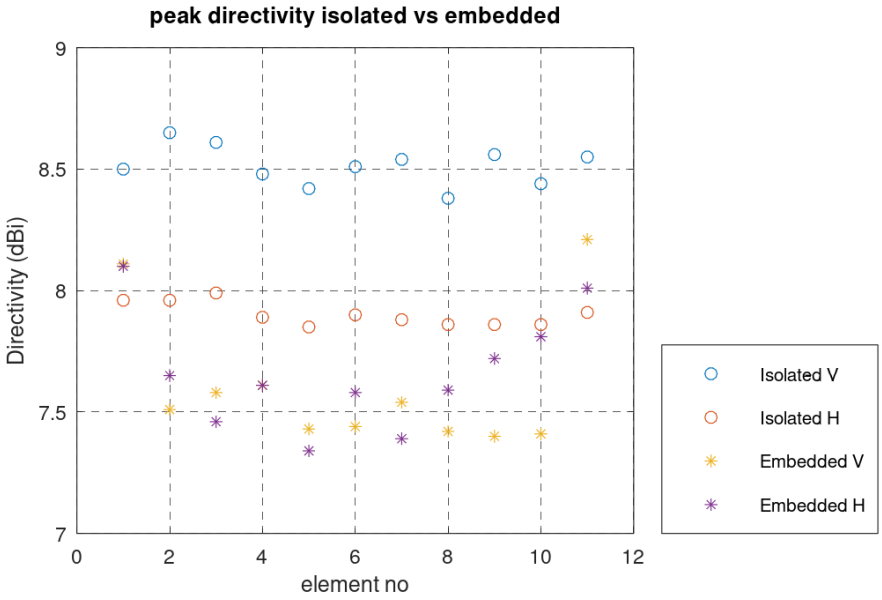

Figure 7-26: Elements positions and peak directivities in the breadboard configuration

The shape of the patterns is affected both in the copolar and the crosspolar, which is also linked to the change in directivity of the ports. The crosspol is affected by the proximity of the elements, principally in the shape of the crosspol and the spatial distribution, while the on-axis value maintains in general very low. The four lobed crosspol pattern that was still noticeable in the individual grounded patterns for PolV is kept, but for PolH is affected and the symmetry of the Xpol lobes is lost. It is recalled that the relative position of the antennas with respect the ground plane is the main cause of the distorted shape of the crosspol with respect an isolated pattern without ground plane or with a centred ground plane.

In the case of the element at the corner of the structure (position #8) the situation is more pronounced due to the double diffraction edges and both copolar and crosspolar patterns are affected but even in this case the directivity of J1 and J2 is within the trend of the other antennas. The crosspolar distribution of this element is more affected.

Both simulation and measurement patterns have been shown to give excellent correlation within the +/-90º range in theta, although the discrepancy in the rear angles (>+90º and <–90º) are larger. It is considered that this is an effect of the differences in the rear side of the 3D EM model and the manufactured setup, as well as the installation on the tower mast of the chamber.

Similarity between patterns and deviation masks have been also shown at the centre frequency. The antennas show an excellent degree of similarity for H and V, in the range of 0.5dB(1σ) in amplitude and 3º(1σ) in phase, even with the effects due to the asymmetry of the array configuration and the different positions of the antennas in the setup, that have been noticed above. It is also noticeable that the effect of coupling between ports makes that H and V patterns show better similarity, and the deviation mask of the combined H-V is similar to that of the isolated H and V polarizations. This is also aligned with the increased similitude of the peak directivity of the H and V ports that has been mentioned.

8. INSTRUMENT PERFORMANCES

With the ALBA antenna patterns, the associated radiometric performances at image reconstruction level were derived by UPC. The target instrument topology was that of the TriHex concept presented in Martin-Neira et al, 2023. TriHex is formed by three hexagonal arrays of 12 antennas per side flying in very close formation and alias-free imaging conditions, achieving a spatial resolution of 15 km at nadir for the SMOS orbit and an alias-free swath of about 1200 km. This large field of view allows for an improvement of the effective radiometric sensitivity. In addition, retrievals for a single hexagon the size of one of TriHex hexagons was also considered in order to compare results.

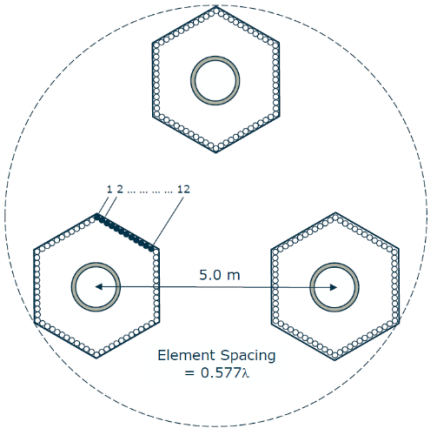

Figure 8-1: TriHex instrument topology (Martin-Neira et al, 2023)

8.1 SYSTEM SIMULATOR DESCRIPTION

A forward and backwards simulation was performed using three sets of antenna patterns as follows, and a full polarization reconstruction was carried out averaging all redundant visibilities over a grid of 128 x 128 points Discrete Fourier Transforms. The spatial components were windowed using a Hamming window.

- Simulated antenna patterns
- Measured antenna patterns at DTU
- Measured antenna patterns at DTU + measurement errors

The following target scenes were simulated and results were analyzed for all datasets.

- An Earth ocean scene including the Fresnel variation with incidence angle in horizontal and vertical polarizations.
- An Earth land scene consisting of a constant scene of 200 K in both polarizations. An Earth mixed scene half of it being ocean, half of it being land, with a realistic coast line separating both parts.

- A point source of 100 K with 0 K background in the centre of the field of view an Earth ocean scene. With a 10000 K point source at the Earth horizon in the along-track direction, to simulate a strong RFI point source.
- An Earth ocean scene with a 10000 K point source at (+0.2, +0.87) in direction cosine coordinates, to simulate the Sun

The incorporation of the simulated and measured antenna patterns in the image reconstruction software required pattern replication and rotation due to the limited set of available patterns.

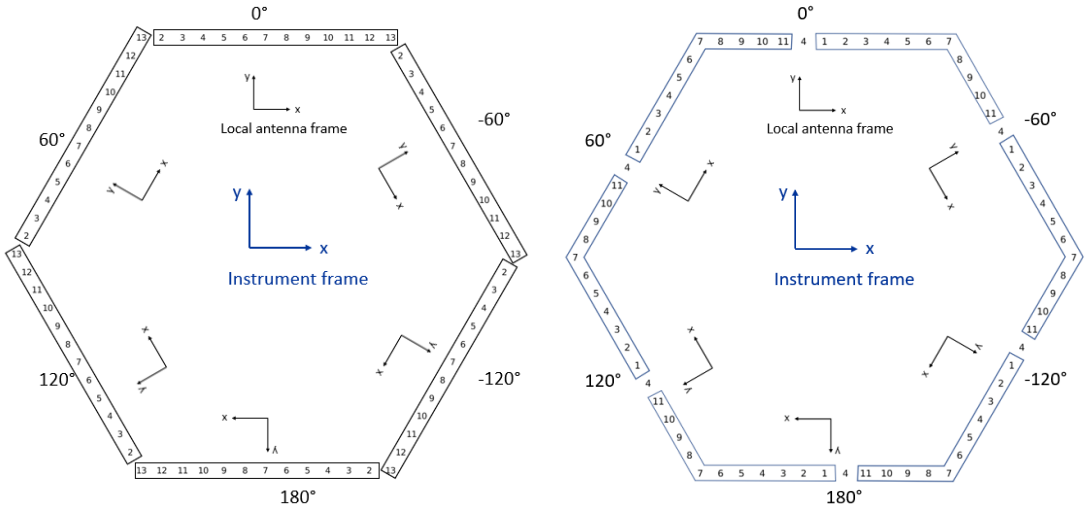

Figure 8-2: Hexagon population and rotation of simulated (left) and measured (right) antenna patterns

8.2 IMAGE RECONSTRUCTION RESULTS

The error performance was assessed for all the cases, with special emphasis on the floor error. Scenes with point sources showed representative results for the sidelobe levels of the instruments with the considered window. Mixed land-sea scenes show transition ripple compatible with the spatial resolution of the instrument.

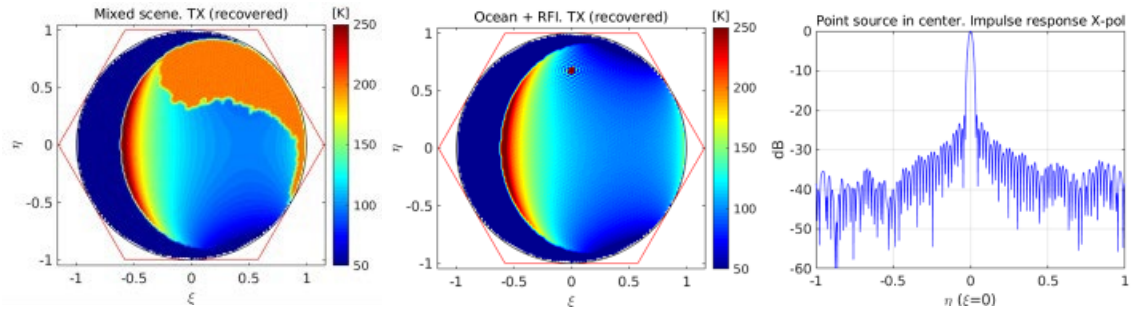

Figure 8-3: Recovered mixed-scene (left), ocean + RFI scene (centre) and impulse response cut (right)

8.2.1 Error-free antenas

Reconstructed images were compared to the original ones, for all synthetic scenes listed earlier. In all the cases the errors are only clearly visible in sharp transitions (e.g., Earth limb), which is due to the finite spatial resolution of the instrument. The impact is stronger for the single hexagon compared to TriHex due to the coarser resolution of the former. Since imaging is alias-free, the Gibbs effect is the only source of discrepancy between the synthetic scene and the reconstructed one. As indicated, Hamming window is used in all cases. The results obtained were essentially the same using either simulated or measured patterns. This is not surprising since a two way forward-backward simulation is a mathematical process that should always be consistent to recover the original data. Only in aliasing situations the use of different antenna sets may have impact since in this case the floor error depends on the similarity between antenna patterns.

A convenient metric to assess the quality of the retrieval is the “floor error”, defined as the difference between recovered and original images of an ocean scene. The following figure shows the floor error found when using measured antennas. Similar images are obtained for simulated ones.

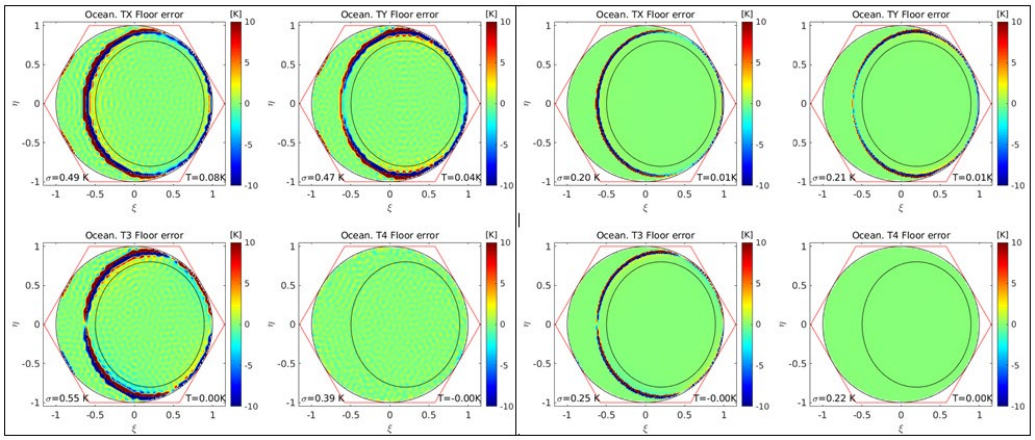

Figure 8-4: Floor error of measured patterns for a single hexagon (left) and the ones of TriHex (right), for H and V polarizations

The numbers at the bottom of each image provide respectively the spatial standard deviation and the mean of the data laying inside the ellipse drawn in black. It corresponds to the 60° incidence angle contour shifted to the left by 0.1 units so as to skip the Earth and unit circle transitions. As a summary, the spatial standard deviations of all cases are given in table. As seen, values are very similar either using simulated or measured antennas. However, they are larger when a single hexagon is considered with respect to the TriHex concept due to the improved spatial resolution of the latter.

Configuration	T_x	T_y	T_3	T_4
Simulated antennas. Single Hex	0.53	0.47	0.62	0.48
Simulated antennas. TriHex	0.19	0.21	0.24	0.22
Measured antennas. Single Hex	0.49	0.47	0.55	0.39
Measured antennas. TriHex	0.20	0.21	0.25	0.22

Table 8-1 Floor error standard deviation

8.2.2 Antenas with measurement errors

The results of the previous section assume that the very same antenna patters are used in the forward model G-matrix and in the one inverted for image reconstruction. In practice, some residual errors are to be expected so that both sets should be in fact slightly different. Errors are here modelled by assuming an additive interfering signal of constant amplitude, this one proportional to the maximum field strength. This would be the case, for example, of a reflection due to finite chamber reflectivity. A mean reflection coefficient of −45 dB is assumed, in line with the DTU facility characteristics, providing an uncertainty around boresight up to about 70° of roughly +/- 0.05 dB. The reconstruction error is computed in the same way as the floor error but using the modified patterns to construct the G-matrix in the forward simulation. The matrix is not inverted again so the original inverted-G matrix is used. The results are summarized in figure below.

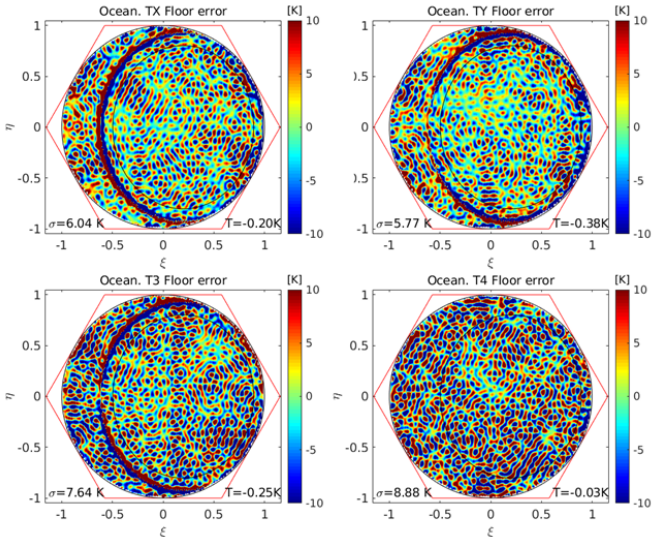

Figure 8-5: Reconstruction error after applying small errors to the antenna patterns

The impact of introducing small errors to the antenna patterns is very large, much more than expected, and larger when considering the TriHex instrument than a single hexagon. To analyze possible causes of this behavior, the condition number of the matrix prior inversion, that is the ratio of maximum to minimum singular values, has been computed. For the measured patterns in a Hexagonal instrument it turns out to be C ≈ 1627, very high and probably the responsible of having unstable inversion. One might argue that replicating identical patterns to populate the instrument may be the reason of having such a large condition number. However, patterns replication using SMOS measured patterns discarded this cause. The only cause that remains for explaining this behavior is the alias-free reconstruction, linked to the fact that the whole unit circle is inscribed in the principal hexagon The obliquity factor becomes singular at the edge of the circle, thus causing the G-matrix elements to be unstable near this zone. This effect has been tried to overcome without success, and further research activities are planned for the future.

9. FINAL CONCLUSIONS AND ACHIEVED RESULTS

This Executive Summary report has presented the work performed by Airbus and UPC in the ALBA antenna project.

The activity includes the design and manufacturing of ALBA antenna element and a test campaign to disclose the performances of the antenna elements both in the RF aspect and in the RF-thermal stability aspect. The design of the antenna is aimed to make a space-flight oriented design, and has been submitted to an extensive functional test campaign in the thermal range with excellent results. The thermal sensitivity of the antennas has been addressed and fulfils the requirements.

As part of the test campaign a breadboard array composed of 11 elements has been also manufactured and tested, in temperature and in RF, and the radiation patterns have been collected. The set of patterns has been used in the simulation of the TriHex Instrument performances.

According to the current TRL definitions following ISO 1620, the activity covered in this project on the antenna for a possible TriHex mission they have been covered TRL4 and TRL5. The test campaign has been focused in functional and performance aspects in ambient and over the temperature, and critical aspects related with the sensitivity of the antenna to the operating thermal requirements (derived from SMOS) have been covered, and it is considered that the level of this antenna design has reached TRL5.

As part of the activity, UPC has developed a software simulator that models the three hexagonal instruments in formation flight having each one 72 dual polarization antennas. The simulated or measured patterns are the information needed to estimate the imaging capability of a complete instrument and determine its performance in terms of spatial resolution, side lobes or floor error, and this has been covered also as part of this project. Two concepts intended to assess in this project were successfully demonstrated through error-free forward-backward simulations: image reconstruction in alias-free condition and polarization rotation of individual antennas in different arms. The first one implies having the unit circle fully inside the fundamental hexagon, and the second means having antennas with unaligned polarization frames. An interesting conclusion is that all results are quite independent of the specific antenna patterns used, either simulated or measured.

10. COMPLIANCE MATRIX

REQ-RE	Parameter	Unit	Requirement	SoC	Comments
10	Bandwidth	MHz	1404 MHz – 1423 MHz	C	section 5.2 in RD5
20	Polarization		Simultaneous Linear H-V	C	section 4.1 in RD5
30	Cross-polarization discrimination	deg	–25 dB (within the HPBW)	NC	For the individual antennas shown in section 5.3 (RD5), the on-axis XPD is always in the range from –30dB to –40dB, and the XPD at EOC is in the range of –20dB to –25dB. This is associated to the edged GP test setup. This also occurs in the embedded arrayed pattern, where Xpol to be affected as shown in Section 0 (RD5). XPD values in the range of –20dB have been measured at EOC. At boresight XPD is always better than –25dB and use to be in the –30 to –40dB range
40	Directivity	Deg	>9 dBi	NC	This topic has been subject of several discussions from the beginning of the project and the measurement results confirm the analyses. In section 5.3 (RD5) are shown the directivities of the isolated antennas that are in the range between 7.6-8.2dBi (boresight), and the arrayed results shown in Section 0 (RD5) indicate arrayed directivity vales in the range of 7.3dBi as expected from the project start.
50	Efficiency	% dB	> 93.5 0.3 dB gain loss	C	Measurements included in section 5.3.5 and 5.7.7 in RD5. Gain/Directivity method has been used.
60	HPBW (Θ3dB)	deg	>65	C	Section 5.3 (individuals) in RD5 Section 0 (arrayed) in RD5
70	Input impedance	Ohm	50	C	
80	Return loss	dB	<–20 Target: –25	C	Section 5.2 in RD5

REQ-RE	Parameter	Unit	Requirement	SoC	Comments
90	Coupling between H-V ports	dB	<–25	C	Section 5.2 in RD5 Section 5.4 in RD5 Section 5.6 in RD5 In all cases requirement refers to the internal H-V coupling between antenna ports, that has been shown to be in the range of –35 to –40dB. Coupling between different elements is associated to spacing that has been updated to 0.577λ and coupling terms have been simulated and measured to be –18dB (V-V) and –25dB (H-H).
100	Phase centre accuracy	deg	0.0037 λ (x-y) 0.015 λ in z axis	C	Word 'accuracy' in this requirement is slightly misleading since it seems to refer more to the method of calculation than to the value itself. In any case the position in local X-Y antenna coordinates is strongly affected by the position of the antenna close to the edge of the structure, and the coupling between elements. Section 5.7.2 in RD5
110	Envelope	mm	0.577λ	C	By design section 5.1 in RD5
120	Mass	g	< 150 Target: 100	NC	NC by 5.7g (excluding attachment screws). Section 5.1 in RD5
130	Ground plane size (stand alone)	cm	90 x 90	C	For individual testing purposes.
140	Ground plane embedded	cm	90	C	
150	Any electrical gap		Closed between the radiating element and ground plane	C	Section 4.1 in RD5 (by design)
160	Temperature range	deg	[–10,+40]	C	Section 5.4 in RD5 Section 5.5 in RD5 Section 5.6 in RD5

REQ-RE	Parameter	Unit	Requirement	SoC	Comments
170	Temperature stability of insertion phase		Amplitude: 0.05 dB stability variation Phase:1 deg stability variation	C	The measurement of stability included in section 5.5 in RD5 indicate amplitude and phase stability in the thermal range of +/-0.025dB and +/-0.5º, compliant to the specification
180	Pattern deviation (TBC)	dB deg	Amplitude: < 0.25 dB for 0° < θ < 35°; < 0.3 dB for 35° < θ < 50°; < 0.5 dB for 50° < θ < 90° Phase: < 0.5° for 0° < θ < 35°; < 1° for 35° < θ < 50°; < 2.5° for 50° < θ < 90°	C	Section 5.3.3 in RD5 shows the individual patterns measured at the edge GP. The 1σ deviation is within requirements for H and V but combined H&V is not, due to different effect of diffraction. Compliance is stated as a guide of the similarity between the different manufactured elements. Section 0 in RD5 shows the arrayed deviation masks for H, V and H&V. It has been remarked that H&V is not similar to H and V alone, but the results are larger than the requirement as result of the combined effect of coupling and diffraction (0.5dB(1σ) in amplitude and 3º(1σ) in phase).
190	H-V pattern similarity (TBC)	dB deg	Amplitude: < 0.25 dB for 0° < θ < 35°; < 0.3 dB for 35° < θ < 50°; < 0.5 dB for 50° < θ < 90° Phase: < 0.5° for 0° < θ < 35°; < 1° for 35° < θ < 50°; < 2.5° for 50° < θ < 90°	NC	Section 5.3.3 in RD5 shows the individual patterns measured at the edge GP. The 1σ deviation for H&V is not compliant due to different effect of diffraction Section 0 in RD5 shows the arrayed deviation masks for H&V. Results are not compliant as explained in previous requirement.
200	Orientation marking		Required to define polarization axis	C	Mechanical design in Section 4.1 in RD5 shows a corner hole that is used to perform polarization alignment in the integration process

END OF DOCUMENT